On the Development of the Wavelength Shifter Deposition System for the DEAP-3600 Dark Matter Search Experiment

by

Benjamin Lowell Broerman

A thesis submitted to the
Department of Physics, Engineering Physics and Astronomy
in conformity with the requirements for
the degree of Master of Science

Queen's University
Kingston, Ontario, Canada
October 2015

Abstract

The DEAP-3600 dark matter search experiment uses 3600 kilograms of liquid argon as a target medium contained in a spherical acrylic vessel. Particle interactions in liquid argon produce vacuum ultraviolet light at a peak wavelength of 128 nanometers, which is not directly visible by the 255 inward-facing photomultiplier tubes. To make visible these interactions, the organic wavelength shifter 1,1,4,4-tetraphenyl-1,3-butadiene, with a re-emission spectrum peaked at 430 nanometers, was evaporatively deposited over the inner surface of the acrylic vessel. The several micron thick coating covers approximately 9 square meters. Application of the coating was performed under vacuum using an evaporation source deployed in the center of the vessel before filling with argon. Research and development on the deployment system for sources inside the acrylic vessel, small scale testing of the evaporation source, and data from test deposition thickness monitoring will be presented, as well as details on the development of the final source, deployment, and performance.

Acknowledgments

I would like to express my gratitude...

- foremost, to my advisor, Mark Boulay, for the opportunity to continue my studies and to work as a member of the DEAP collaboration.

- to Marcin Kuźniak, with whom I worked most closely on this project, for his time and effort in dealing with my numerous questions, and at times outlandish ideas.

- for the technical support from Koby Dering, Rob Gagnon, Peter Skensved, Tony Flower and those underground with whom I worked alongside.

- for the numerous drinks with Mark Ward, Pietro Giampa, Satoko Asahi, and Efthymios Koniaris.

- to my parents, Ralph and Andrea, for instilling a creative, yet technical eye and to Katie and Robert, for all your support during my studies.

- lastly, to Frank Mead, who continues to be an inspiration.

Thank you.

Ben

October 2015

Statement of Originality

DEAP-3600, like most modern particle physics experiments, cannot come to completion solely, but is the result of much collaborative effort. The work described in this thesis is original and was conducted by the author. When necessary, credit is explicitly noted for those who made significant contributions to the work.

Extensive, collaboration-wide effort was expended in the preparation and construction of the TPB deposition system underground under the management of T. Flower, and in remote monitoring during the bakeout of the acrylic vessel. Prototyping of the initial TPB source was done by T. Pollmann based conceptually from M. Boulay and work from C. Gilmour. Design and specification of the initial deployment system was outlined by S. Florian and M. Kuźniak. Welding of the TPB source was done by C. Hearns. Code for the analysis of RGA data was developed by M. Ward. The fast LED pulser was donated from L. Thompson. Extensions and finalizations, building on these previous works, was performed by the author.

Table of Contents

List of Tables

List of Figures

List of Acronyms

5WC 5-way cross

AV Acrylic Vessel

CF Conflat

PE Photoelectron

PMT Photomultiplier Tube

PSD Pulse-shape Discrimination

RGA Residual Gas Analyser

RTD Resistance Temperature Detector

TPB 1,1,4,4-tetraphenyl-1,3-butadiene

UPW Ultra-pure Water

VUV Vacuum Ultraviolet

WIMP Weakly Interacting Massive Particle

Chapter 1

Dark Matter

Zwicky's observations in the 1930's indicated a mismatch in the accountable mass inside the Coma cluster when compared to the recorded radial velocities [1] [2]. The velocity dispersion was observed to be too high for the galaxy cluster to be bound gravitationally by its own apparent mass. The postulation was then that a unobservable, non-luminous (dark) mass was distributed throughout the galaxy cluster contributing to its velocity distribution.

Results from the PLANCK survey support a cosmological model, ΛCDM, which delineates 68.5% of the mass-energy density of the universe to dark energy, 26.6% to cold dark matter, and 4.8% to ordinary matter [3]. The largest component, dark energy, is responsible for the acceleration and current expansion of the universe. The smallest component is left for the known, visible matter.

1.1 Dark Matter Candidates

There have been proposed many hypothetical models to populate the dark matter contribution of ΛCDM [4]. However, there are certain criteria a viable dark matter particle must fulfill. The candidate particle should be:

Massive The candidate particle should interact gravitationally (i.e. have mass) to account for the discrepancies in galactic rotation curves.

Stable The candidate particle should be stable, or have a decay time that is on order the age of the universe. If this were not the case, then the particle would have already decayed away, making its detection impossible.

Non-relativistic The candidate particle should be non-relativistic (cold). It is only simulations of cold dark matter that provide a reasonable fit to the large-scale structures in the universe [5].

Electrically Neutral The candidate particle should not participate in electromagnetic interactions. If the particle coupled electromagnetically its presence would have likely been directly observed in interactions with the photon.

Among the leading candidates for a dark matter particle is the Weakly Interacting Massive Particle (WIMP) with predicted masses on the order of GeV/c^2 to TeV/c^2, interaction cross sections less than 1 picobarn, and a local density of 0.3 GeV/cm^3 [6].

1.2 Expected Signal

Dark matter can potentially be detected through its recoil off target nuclei. The WIMP-nucleon cross section for a momentum transfer q can be written as:

$$\frac{d\sigma(q)}{dq^2} = \frac{1}{4\mu^2 v^2}\sigma_0(q)F^2(q) \tag{1.1}$$

for v the velocity of the dark matter particle in the lab frame, $\mu = M_\chi M_A/(M_\chi + M_A)$ the reduced mass of the dark matter (M_χ) and target nuclei (M_A) system,

nuclear form factor $F(q)$, and momentum independent cross section σ_0, which for spin independent interactions is:

$$\sigma_0^{SI} = \frac{4\mu_A^2}{\pi}[Zf_p + (A-Z)f_n]^2 \tag{1.2}$$

for A the atomic mass of the target nuclei, Z proton number, μ_n the reduced mass of the WIMP-nucleon system, and $f_p(f_n)$ the spin independent WIMP-proton(neutron) coupling strengths. In principle, the WIMP-nucleon cross section may also have a dependence on the spin on the nucleon, in which case the spin-dependent cross section contribution is:

$$\sigma_0^{SD} = \frac{32G_F^2\mu_A^2}{\pi}\frac{J+1}{J}(a_p\langle S_p\rangle + a_n\langle S_n\rangle)^2 \tag{1.3}$$

for G_F the Fermi constant, J total nuclear spin, $a_p(a_n)$ the spin-dependent WIMP-proton(neutron) coupling strength, and $\langle S_p\rangle(\langle S_n\rangle)$ the expectation value of the proton(neutron) spins within the nucleus [7].

The predicted observable signal in a laboratory experiment is a featureless exponential rise in the low energy nuclear recoil spectrum, with the differential recoil spectrum taking the form:

$$\frac{dR}{dE_R} = \frac{R_0}{E_0 r}exp(-E_R/E_0 r) \tag{1.4}$$

for E_R the recoil energy, E_0 the incident kinetic energy for a dark matter particle of mass M_χ, r a kinematic factor equal to $4M_\chi M_A/(M_\chi + M_A)^2$ for a target nuclear mass M_A, R the event rate per unit mass, and R_0 the total event rate [8].

1.3 Current Status of Direct Dark Matter Searches

Despite much experimental effort searching for a direct dark matter signal, there is yet no conclusive evidence to its detection. Claims of a signal from low mass WIMPs (∼10 GeV) by the NaI-based DAMA/LIBRA experiment [9] are in strict disagreement with exclusion limits from other experiments. The origin of the signal seen in DAMA is not understood, though many potential explanations (for example a muon-induced background [10]) have been proposed. Current world limits on spin independent dark matter interactions are held by the liquid xenon-based LUX experiment and can be seen in Figure 1.1.

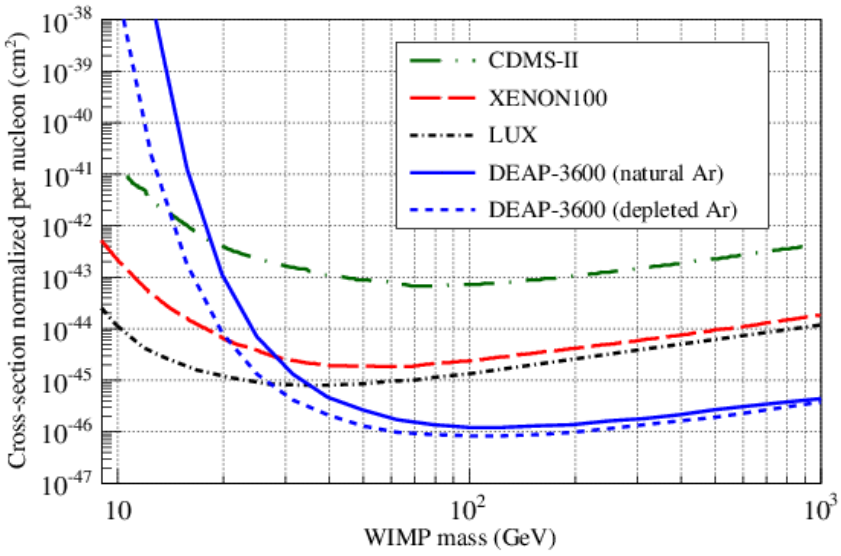

Figure 1.1: Dark matter parameter space in mass and cross section. Plotted are the leading limits from LUX, XENON100, and CDMS as well as the projected sensitivity for DEAP-3600 with natural and depleted argon (M. Kuźniak).

Chapter 2

DEAP-3600

The Dark Matter Experiment using Argon Pulse-shape Discrimination (DEAP) is a single phase liquid argon dark matter search experiment. In a single phase noble liquid experiment, an incident particle interacting with (transferring energy to) the target nuclei generates a scintillation signal. This signal is dependent on the type of interaction and can be used to distinguish known electromagnetic background events from nuclear recoil events, the latter of which is expected for dark matter interactions. The experiment is in the final stages of construction in the Cube Hall of SNOLAB in Sudbury, Canada [11], which as an experimental site, provides a 6000 meter water equivalent overburden to reduce the flux of cosmic-origin backgrounds. Specifically, the cosmic ray muon flux is reduced to 0.27 μ m^{-2} day^{-1} [12]. DEAP-3600 is the next generation experiment following the prototype DEAP-1 detector and builds upon the techniques presented in [13].

2.1 Construction

DEAP-3600 is shown schematically in Figure 2.1 and specifications to its design can be found in [14]. 3600 kilograms of liquid argon (1000 kilograms fiducial mass) is

contained in an acrylic vessel (AV) 85 cm in radius. Cylindrical light guides, 50 cm in length, couple to 255 8 inch Hamamatsu R5912 HQE photomultiplier tubes (PMTs). All PMT cables are brought through sealed flange feedthroughs on the central support assembly just below the deck, and routed to the nearby electronics racks. Multi-layer high density polyethylene (HDPE) and foam filler blocks occupy the space between light guides to provide neutron moderation and thermal insulation. A 3 meter coaxial neck joins the acrylic sphere to the supporting deck above; the outer layer of the neck provides mechanical support while a vacuum jacked inner neck completes the cryogenic volume of the detector. The argon in the vessel is maintained near 87 K with a liquid nitrogen cooling coil installed inside the neck. A stainless steel pressure vessel encapsulates the fully populated AV, which is further placed in an 8 meter diameter water tank instrumented with PMTs serving as a muon veto.

At the top of the neck is a glovebox providing inlets and outlets for the liquid nitrogen and argon lines. Final inner-detector construction tasks were performed using this glovebox as a buffer between the clean acrylic vessel and lab air, and was continually purged with radon-scrubbed boil-off nitrogen. All work inside the glovebox is done through 6 gloveports fitted with low radon emanation butyl rubber gloves. A large gatevalve allows entry into the glovebox for installation of larger items, which during construction was coupled to a large stainless steel canister.

After construction and population of the AV, a robotic sander (the resurfacer) was deployed in the vessel. Although special care was taken during the manufacturing of the acrylic to keep uranium and thorium concentrations to a minimum, these species will still be present in all components of the detector. Both ^{238}U and ^{232}Th isotopes have very long half lives and present a continuous source of potential backgrounds

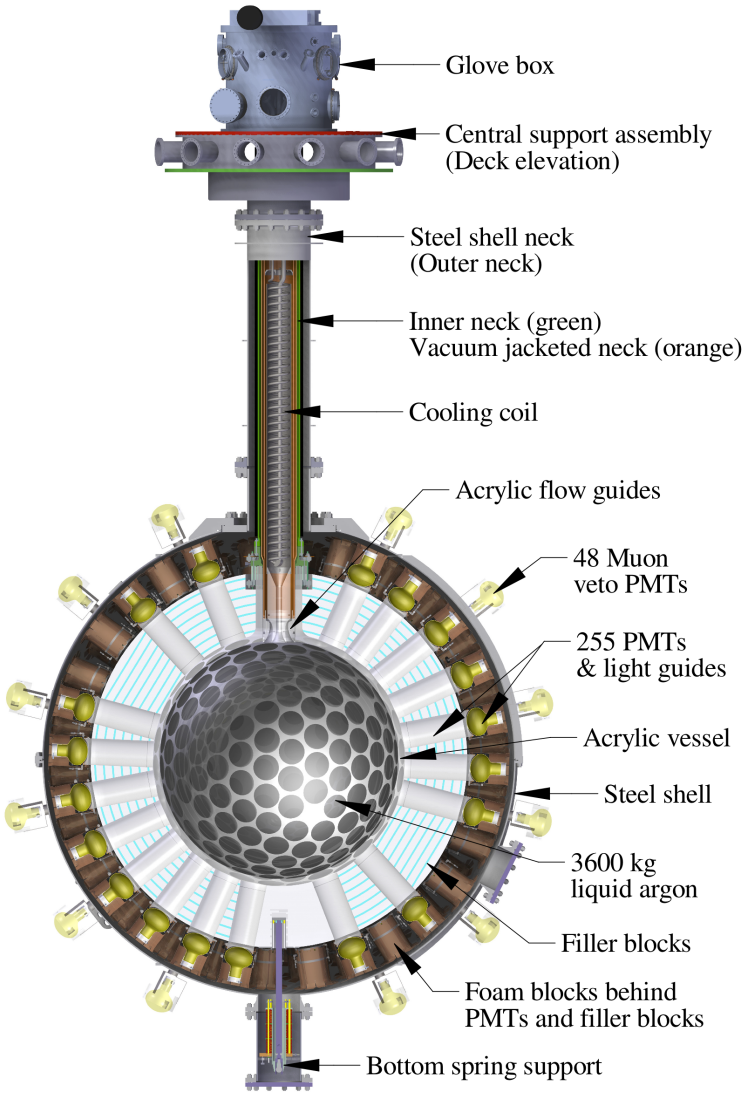

Figure 2.1: Schematic of the DEAP-3600 detector. The 85 cm radius acrylic vessel contains 3600 kg of liquid argon and is viewed by 255 PMTs. HDPE and foam filler blocks provide thermal and neutron moderation. A stainless steel shell encapsulates the vessel.

over the lifetime of the experiment. The full decay chain from ^{238}U is shown in Figure 2.2.

Both neutrons and alphas pose difficult backgrounds for DEAP (the handle on electromagnetic events will be discussed in Section 2.2.1). Neutrons can be largely

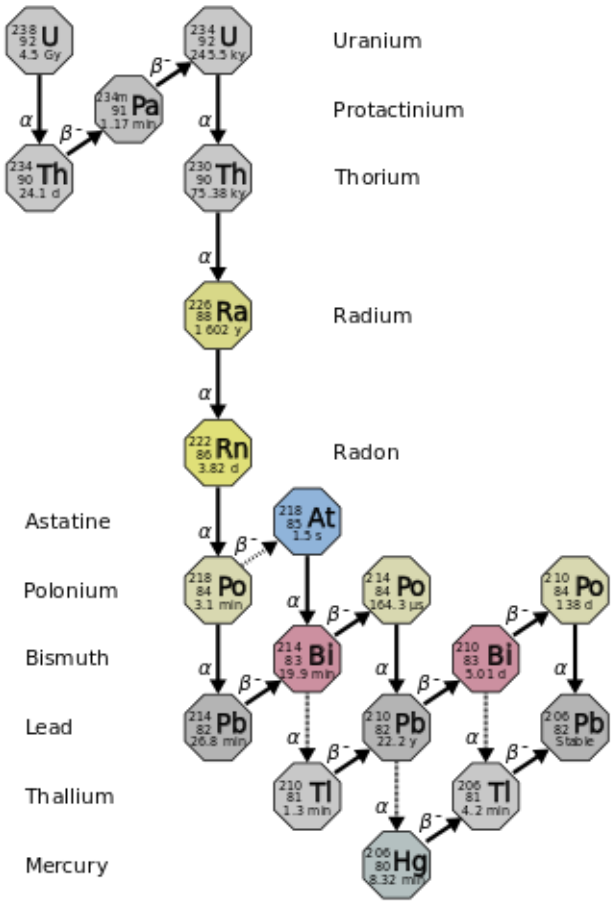

Figure 2.2: Uranium Decay Chain. (Wikipedia)

mediated away, though are problematic as they are massive, have no charge, and can induce an argon nuclei recoil signature very similar to that as expected for dark matter interactions. Neutrons will often interact more than once inside the target volume, though, which is not expected for dark matter. The remaining alpha background can be separated into intrinsic and acquired contamination. Strict material selection, keeping the uranium and thorium contents low, can reduce the intrinsic radio-background. The acquired contamination can be reduced by limiting the exposure of the most sensitive detector components to air. Radon in the air can diffuse

into the acrylic, for example, and implant alpha emitters. The energy spectrum, if the alpha in these implanted decays loses energy exiting the acrylic and deposits only a fraction of its total energy in the argon volume, can leak into the energy region of interest for the dark matter search. In order to achieve the background levels from radio-purity requirements, it was required that the resurfacer sand off approximately 1 mm of acrylic from the inner surface to remove contaminants, mainly from polonium and lead isotopes, which result from decaying diffused-in radon.

After resurfacing, during which the AV was continually flushed with ultra pure water (UPW), radon-scrubbed boil-off nitrogen was flowed into the detector as purge gas while preparations for the vacuum and wavelength shifter deposition systems were set up. A heating source was deployed at the center of the AV (further discussion in Chapter 5) to perform a vacuum bake; this outgases much of the water that was absorbed by the AV during resurfacing. Additionally, species other than argon (water), can lead to quenching of the light from the argon emission process [15]. A vacuum deposition of the organic wavelength shifter 1,1,4,4-tetraphenyl-1,3-butadiene (TPB) was then performed over the spherical inner AV surface. The need for this coating will be discussed in Section 2.2, and details of its application will be discussed in Chapter 3.

Before the final installation of the cooling coil and flow guide, the deployment system was used to lower an optical calibration source, the LaserBall, which provides a fast, triggered light source at 375 nm, 405 nm, and 445 nm. Early optical analyses are ongoing with this data.

2.2 Optical Processes

There are two main optical processes that occur before the information on the deposition of energy from an event can be registered by the PMTs: initial argon scintillation followed by wavelength shifting from TPB.

2.2.1 Argon Scintillation

The underlying scintillation mechanism is similar to that in all liquid noble gas experiments, though specifically a treatment for argon will be presented. As a target medium, liquid argon is advantageous. It is relatively inexpensive, easy to purify, and possesses high light yield and useful pulse shape discrimination (PSD) characteristics [16]. Table 2.1 lists some characteristics of two noble gases used in dark matter experiments.

Parameter	Ar	Xe
Atomic Number Z	18	54
Atomic mass A	40.0	131.3
Boiling Point (K)	87.3	165.0
Light Yield (photons/MeV)	40 000	42 000
Peak Scintillation Wavelength (nm)	128	174
Prompt time constant τ_1 (ns)	6	2.2
Late time constant τ_3	1.59 μs	21 ns
I_1/I_3 for electrons	0.3	0.3
I_1/I_3 for nuclear recoils	3	1.6

Table 2.1: Characteristics of argon and xenon relevant for dark matter search experiments. The large difference between the prompt (singlet) and late (triplet) lifetimes in argon is what provides the pulse shape discrimination between electromagnetic events and nuclear recoil type events [13] [17].

The peak emission from argon scintillation is in the vacuum ultraviolet range (VUV) at 128 nm. This fluorescence from interactions in liquid argon results from

de-excitations of dimer molecules, bound two-atom states, and not from individual atoms. After the creation of an excited or ionized argon atom due to incident radiation, dimer formation can occur with a neighboring ground state argon atom.

There are two paths, Equations 2.1 and 2.2, that this overall reaction may take, the choice of which is dependent on the type of incident radiation. It is possible for nuclear and electromagnetic recoil events to both create singlet and triplet dimer states, however the intensity of singlet to triplet state production for initial nuclear and electromagnetic recoil events is different, as can be seen in Table 2.1. If the event is nuclear recoil like, the initial argon atom is likely excited and primarily forms a dimer molecule in the singlet state with a prompt lifetime of 6 ns. WIMP dark matter is expected to produce a nuclear recoil signal. If the event is electromagnetic in nature, the initial argon atom is likely ionized and forms a dimer molecule in the triplet state, with a lifetime of 1.6 μs.

Excitation: Ar^*

$$\begin{aligned} Ar^* + Ar + Ar &\rightarrow Ar_2^* + Ar \\ Ar_2^* &\rightarrow 2Ar + \gamma \end{aligned} \tag{2.1}$$

Ionization: Ar^+

$$\begin{aligned} Ar^+ + Ar &\rightarrow Ar_2^+ \\ Ar_2^+ + e^- &\rightarrow Ar^{**} + Ar \\ Ar^{**} &\rightarrow Ar^* + \text{heat} \\ Ar^* + Ar + Ar &\rightarrow Ar_2^* + Ar \\ Ar_2^* &\rightarrow 2Ar + \gamma \end{aligned} \tag{2.2}$$

The subscript 2 in Equations 2.1 and 2.2 denote the dimer state and the gamma in the final state is the 128 nm VUV photon. The first step in Equation 2.1 and fourth step in Equation 2.2 occur as three-body collisions. The "heat" in step 3 of 2.2 refers to a non-radiative transition dissipating energy to vibrational modes [18] [19]. The dimer formation from incident radiation provides the needed Stokes shift (separation in the emission spectrum from argon dimer molecules to that of the absorption spectrum of argon atoms) to allow the final state 128 nm gamma to traverse the argon volume. Without this shift in the emission and absorption spectra, the emitted gamma would be immediately absorbed, and the information about the event would not be transmittable.

The strong dependence on the type of incident radiation and subsequent dimer state lifetime can be exploited in pulse shape discrimination. By looking at the amount of prompt and late light of a recorded event, identification of the initial type of interaction (electronic or nuclear recoil) can be determined. The discrimination variable is F_{prompt}, a ratio of the number of photoelectrons (PE) in the prompt window of a pulse (50 ns before the peak to 150 ns after the peak) collected over each PMT,

to that of the total recorded number of PE for a waveform.

Electronic recoils from β/γ events constitute the majority of potential background events in DEAP-3600, the origin of which must be understood and identified; specifically, beta decays from cosmogenically produced ^{39}Ar dominate the expected background. With this definition of F_{prompt} nuclear recoil events, as expected for dark matter interactions, would have higher F_{prompt} values than electronic recoil events. With a low F_{prompt} analysis cut, the separation of known β/γ background events can be made. Misidentification of β/γ events in the energy region of interest for an expected dark matter signal is estimated from DEAP-1 data to be less than 2.8×10^{-8} (further information on the use of PSD for DEAP-1 can be found in [20] and [21]).

2.2.2 Wavelength Shifting

Vacuum ultraviolet (VUV) photons, as of the emission products from argon dimers, are absorbed by most optical media like quartz and acrylic, making signals difficult to directly propagate from the argon volume to the PMTs [22]. 1,1,4,4-tetraphenyl-1,3-butadiene, the wavelength shifter used in DEAP-3600, absorbs ultraviolet light and re-emits at visible wavelengths with a singlet re-emission time of order one nanosecond [23] [24]. The chemical formula for TPB is $(C_6H_5)_2C{=}CHCH{=}C(C_6H_5)_2$ and its molecular structure is shown in Figure 2.3.

Fluorescence, which results from molecular de-excitations on nanosecond time scales, can be represented by example with the energy level diagram in Figure 2.4. For TPB, the four benzene rings seen in Figure 2.3 provide the π-electrons due to overlapping $2p_z$ electron orbitals from the carbon atoms that are perpendicular to the plane of the carbon ring. When the molecule is excited from ultraviolet radiation

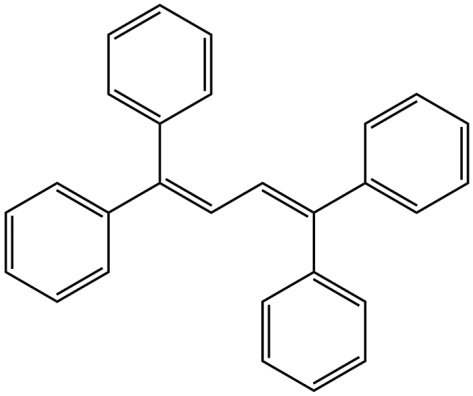

Figure 2.3: Structure of the TPB molecule

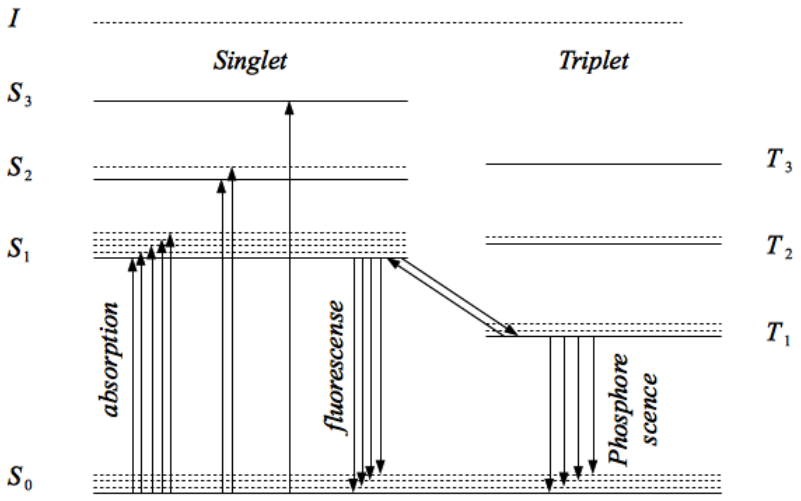

Figure 2.4: π-electronic state diagram for benzene.

(photoluminescence), there is an electronic transition from the ground state to one of the excited singlet states.

Each electronic level is made up of vibrational and rotation sub levels. The energy spacing of adjacent rotation levels can be 0.01- 0.001 eV, while the vibrational levels is on the order of 0.1 eV [25]. Transitions resulting in fluorescence occur mainly

from the π-electrons in the zero vibrational state. This can be seen from Boltzmann statistics where the population of molecules in state 1, n_1, relative to that of state 0, n_0, is given by:

$$n_1 = \frac{n_0 g_1}{g_0} exp(\frac{-\Delta E}{k_B T}) \tag{2.3}$$

where g_1 and g_0 are the degeneracies of the energy levels, k_B Boltzmann's constant, and ΔE the energy (sub)level spacing. As an example, for typical vibrational level spacing and like-degeneracies, the population n_1 can be on order 10^{-2} that of n_0, which indicates the majority of state population is in the zero vibrational states for the de-excitation.

Excitation raises the electron from the ground state to one of the vibrational levels S_1. Electrons in higher vibrational levels quickly relax to the lowest vibrational state in that level through collisions with neighboring atoms. Furthermore, there is no transition from S_2 to S_0 due to picosecond internal conversion from S_2 to S_1. The emission from one of the excited energy levels to one of the ground state vibrational levels results in a spectrum for TPB peaked at 430 nm, as shown in Figure 2.5.

Figure 2.5 shows the TPB emission spectrum from [22] and a typical PMT quantum efficiency curve for the Hamamatsu R5912 PMTs. The emission spectrum falls in the peak of the quantum efficiency of the PMTs, and therefore adequately completes the transmission of event information.

The use of a wavelength shifter has implications on the PSD by broadening in time the signal viewed at the PMTs. This broadening expands the late time emission profile of the signal while minimally altering the prompt signal region. With a fixed pulse window, this would potentially lead to greater late light being collected, thereby

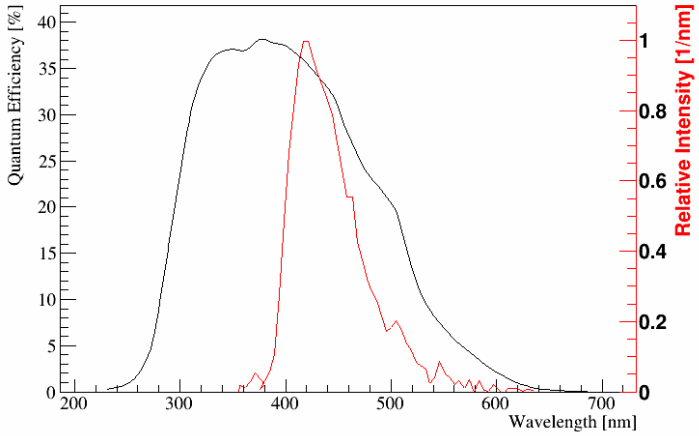

Figure 2.5: Typical PMT quantum efficiency curve for the R5912 HQE PMTs and the emission spectrum from TPB. The alignment of the two curves allows the event information from argon dimer to be read out by the PMTs. The TPB emission spectrum has been arbitrarily normalized to the peak height of the PMT quantum efficiency curve.

driving down the F_{prompt} value for a given signal. This could lead to a misidentification of nuclear recoil events as background electromagnetic events. Investigating this broadening and its effect on the PSD is ongoing.

2.3 Physics Goals

DEAP-3600 will perform a spin independent dark matter search targeted at a WIMP-nucleon cross section of 10^{-46} cm^2 for a 100 GeV/c^2 WIMP mass. Within a few months of data taking, it should have a dark matter sensitivity surpassing that of current world limits. The expected sensitivity plot can be seen in Figure 1.1 for no dark matter events seen and no background in a 3 tonne-year exposure with both natural argon (solid blue) and depleted argon (dashed blue) which has a lower content

of the beta decay isotope ^{39}Ar.

Chapter 3

TPB Deposition System

The purpose of the deposition system is to deposit a coating, several micrometers thick, over the interior of the AV of the wavelength shifter 1,1,4,4-tetraphenyl-1,3-butadiene. This coating absorbs ultraviolet light resultant from particle interactions in liquid argon, and re-emits the light in the visible range, making visible the interactions inside the target volume to the PMTs.

3.1 Principle

The principle of the deposition system is to allow TPB molecules to sufficiently scatter inside a perforated spherical source such that when the molecules do find one of the exit holes, they are traveling with a random trajectory; the molecules have no memory of their initial location after leaving an inner crucible. In effect, this creates multiple evaporation point sources, each covering a region of the inner AV surface. Integrating over all the exiting trajectories would leave a uniform distribution of TPB molecules incident on the inner surface of the acrylic vessel. There are a number of tunable parameters in the calculation of the exiting hole sizes, which must maintain the proper balance between the generation rate of the TPB gas and emission rate from

the source.

Generation of the TPB gas is driven by heating the exterior of the metal source to around 208°C, the sublimation temperature of TPB. A cylindrical copper crucible with dimensions 34 mm by 35 mm, into which the TPB powder is loaded, hangs inside the source which is radiatively heated from the surrounding shell. When evaporation begins, the molecules scatter inside the source, adsorbing on the inner shell surface if incident and immediately desorbing, until finding one of the twenty holes.

TPB deposition rates performed on the test vessel at Queen's, as will be discussed in Chapter 5, ranged from 1 μm/hour to 5 μm/hour. The deposition rate for the coating on the DEAP-3600 acrylic vessel, discussed in Chapter 6, reached a stable maximum of 0.25 μm/hour.

The total mass being deposited on the inner surface of the AV per second is given by the product of the AV surface area, deposition rate, and density of the TPB layer:

$$R_{dep} \times A_{AV} \times \rho \tag{3.1}$$

for R_{dep} the final rate, $A_{AV} = 9.10$ m^2, and $\rho = 1.079$ g/cm^3. This leads to a deposition rate of 6.9×10^{-7} kg per second or 1×10^{18} molecules per second for an approximate mass of the individual TPB molecule of $6{\times}10^{-25}$ kg.

Making the mean free path of the TPB molecule sufficiently small to ensure scattering inside the source and random exiting trajectories, a pressure inside the source must be maintained following:

$$p = \frac{R_a T}{\lambda \sqrt{2} \pi d^2 N_a} \tag{3.2}$$

for R_a the gas constant equal to 8.314 $m^3PaK^{-1}mol^{-1}$, T the temperature (473 K), λ the mean free path, d the largest diagonal span of the TPB molecule equal to 1220 pm, and N_a Avogadro's number [26]. Taking the mean free path to be one tenth the radius of the TPB source, this leads to a pressure that must be maintained of 0.18 Pa. Using the ideal gas law, the number of TPB molecules required to maintain this pressure is:

$$N_p = \frac{pV}{k_B T} \tag{3.3}$$

for p the pressure, V the volume of the TPB source (for 0.055 m radius source this is 6.97×10^{-4} m^3), k_B the Boltzmann constant in J/K, and T the temperature (473 K). To maintain 0.18 Pa pressure requires 1.92×10^{16} TPB molecules.

Finally, to maintain the random scattering of TPB inside the source, the number of molecules leaving the source (that is the number being deposited on the inner AV surface) must be less than or equal to the evaporation rate from the crucible inside the source. The number of molecules leaving the source is equal to the number of molecules required to maintain the correct pressure in the sphere whilst scattering and hitting an area A_h (the exit hole area):

$$\frac{N_{exit}}{t} = \frac{1}{6}\frac{N_p}{V}\langle v\rangle A_h \tag{3.4}$$

for N_{exit} the number of TPB molecules leaving the source on route to the inner surface of the AV, and $\langle v\rangle$ the average velocity of the TPB molecule (166.5 m/s). Balancing Equations 3.2, 3.3, and 3.4, the total hole size, A_h may be calculated.

3.2 Source Construction

The prototype source was constructed by T. Pollmann, details of which can be found in [27]. Table 3.1 lists the main parameters of the prototype source, as well as final stainless steel version. This first source was made from aluminum which is largely recycled, and often high in uranium and thorium content. The final version of the source was made of as radio-pure components as possible, as it was put inside the acrylic vessel post resurfacing.

Prototype Source	material heating element diameter hole diameter	aluminum Kapton-Nichrome wire/Watlow heater 11 cm 13 mm
Final Source	material heating element diameter hole diameter	304 stainless steel Watlow heater 11 cm 14 mm

Table 3.1: Physical parameters of the TPB sources

The initial aluminum prototype source, shown in Figure 3.1 used Nichrome wire wrapped around the outside of the stainless sphere. The Nichrome wire was encapsulated in Kapton tape to provide electrical insulation while maintaining heat transfer. After test depositions with the prototype source, charing of the Kapton tape was noticed in regions where the Nichrome wire was bent. Although Kapton itself is rated for +400°C, it was speculated that high local heat loads from the Nichrome wire, which was run to approximately 200°C for TPB deposition, may have exceeded the temperature limit for the adhesive backing on the Kapton tape. The annotation in Figure 3.2 highlights this charring of the Kapton tape.

A new heating wire, Watlow 125CH93A1X, was then installed, shown in Figure

Figure 3.1: 11 cm in diameter prototype aluminum TPB source with Watlow heating wire wrapping the outside.

3.1. Here, a Nichrome coil is encapsulated in an outer stainless steel sheath and insulated with Mg0. As there is no electrical contact from the inner heating wire to the exterior of the element, no Kapton wrapping was necessary. The 50 Ω Watlow heating coil is capable of 1 kW heating, but was driven at 120 V limiting the max heating power to 275 W.

Several companies specializing in the production of hollow stainless steel spheres and hemispheres were contacted for the production of the final source. Three 12 cm stainless spheres were ordered from Mao Ping Industrial Co. in Shenzhen, China. One prototype source was created using these spheres. It was noticed that the sphere was formed by welding two separate hemispheres together. After contact with the

Figure 3.2: The prototype aluminum source with original Nichrome wire wrapped in Kapton tape for insulation. Charring, visible by the dark discoloration in the yellow Kapton tape, is highlighted by the red circle.

company, it was unclear of the purity of the weld material used. Non-thoriated welding rods were extensively studied for DEAP and determined to be clean; details can be found in [28]. Because of this, custom 11 cm hemispheres were machined from 304 stainless steel and welded into a sphere with the use of a stainless equatorial joining band. The welding used Blue Demon 2% ceriated tungsten electrodes. A mapping of the hole positions was created and printed as a mask that fit over the outside of the sphere, after which the hole positions were marked with a center punch, then drilled using a step bit. Limitations in the machining method for the holes left only discrete hole sizes possible. The final hole size was machined to be 14.3 mm (9/16") diameter. The final source can be seen in Figure 3.3.

Figure 3.3: Final stainless steel TPB deposition source. The Nichrome wire is held in thermal contact with the stainless steel sphere by compressed stainless tabs. A stainless top hat was machined from which the copper crucible was attached.

For the prototype, extra wire leads were wrapped around bolts in the aluminum sphere to tie the heating element to its surface to maintain good thermal contact. In the final stainless version of the source, thermal contact through brazing the stainless heating wire to the stainless sphere was considered. However, the heat load from the welding tip was high enough to burn through the sheathing on a test Watlow heating wire. Final thermal contact was achieved by bending stainless clips over the coil heater that were affixed with bolts to the sphere surface.

3.3 Instrumentation

The TPB source was specified to be instrumented with a variety of power, signal, and monitoring cables. All cables are brought out of the vacuum space using commercially available vacuum feedthroughs installed on the deployment system. Details of the deployment system will be discussed in Chapter 4.

3.3.1 Source Instrumentation

Power

Power is delivered to the heating element on the TPB source using two cables carrying line level (120 V) voltage. The duty cycle of this applied voltage is varied to control the power to the heater. Additionally, these cables were to be used for the initial optical calibration LED ball to deliver a 0-30 V DC signal which controls the overall intensity of the source.

Triggering

An RG178 50HCX-18 coaxial cable with Pasternack 10-32 cable ends was used for signal readout. Triggering of two mounted LEDs on the TPB source was proposed and developed for monitoring the thickness of the applied TPB coating in situ. This cable was also specified initially to be used as a trigger for both proposed optical calibration sources (LaserBall and UV LED ball). Additionally, the quartz monitor used for direct TPB thickness measurement was read out with this type of cable.

Temperature

To monitor the temperature of the source, two F3105 Thin Film Resistance Temperature Detectors (RTDs) were attached: one on the exterior of the sphere near the heating element, and on one on the copper crucible hanging inside the source. These temperature sensors were initially readout with a LakeShore 218 temperature controller and logged via LabView. The LabView program would use the temperature information to control the duty cycle of the overall heating element by sending a signal to a Watlow DIN-A-MITE Style A solid state relay. The relay and power control for the heater were contained in a ESA approved control box. A 0-10 V control signal would be sent from the LabView computer interface and proportionally converted to a 4-20 mA signal, before being fed into the DIN-A-MITE relay.

3.3.2 Detector Instrumentation

Inner AV Temperature

An Omega OS36 infrared temperature sensor was deployed in the neck of the detector, hanging inside the AV sphere and facing the inner surface. From this the temperature

of the inner surface of the acrylic vessel can be determined without physical contact. To prevent stresses in the acrylic, especially around the neck region, the inner surface of the acrylic was not to exceed 50°C.

Direct TPB Thickness Monitoring

The initial target thickness for the coating on the AV was set at 1 μm. At the intersection of the sphere and neck, an Inficon quartz deposition monitor was deployed to directly measure the thickness of the applied coating. This data is readout using an Inficon SQM-242 Thin Film Deposition Controller Card and logged with LabView software. The monitor operates by measuring the change in the resonant frequency of a quartz diaphragm due to buildup of deposited mass. At discrete frequencies electromechanical resonances exist in the quartz diaphragm. As mass is deposited on the crystal, these frequencies begin to shift downward following [29] [30]:

$$\Delta f = -\frac{f_q^2}{N\rho_q A} M_f \tag{3.5}$$

for f_q the nominal resonant frequency of the crystal prior to coating, N the frequency constant for the specific quartz cut ($\sim 1.67 \times 10^{-3}$ Hzm), ρ_q the density of quartz, A the coated surface area, and M_f the deposited mass.

The final coating thickness read from the Deposition Controller Card is calculated from Formula 3.6 [31]:

$$T_f = \frac{Z_q \times 10^4}{2\pi z \rho}\Big\{\frac{1}{F_{co}} arctan(z\, tan(\frac{\pi F_{co}}{F_q})) - \frac{1}{F_c} arctan(z\, tan(\frac{\pi F_c}{F_q}))\Big\} \tag{3.6}$$

for T_f the thickness of the deposited film in kÅ, F_{co} the starting frequency of the quartz crystal (Hz), F_c the final frequency of the quartz crystal (Hz), F_q the natural crystal frequency equal to 6.045 MHz, z the Z-ratio of the deposited film which is a measure of the acoustic impedance of the film (here set to unity), Z_q the specific acoustic impedance of quartz equal to 8.765 MHz, and ρ the density of the deposited film in g/cc.

Indirect TPB Thickness Monitoring

It is desirable to create a mapping of the uniformity of the TPB coating over the entire surface of the AV, as the optical response of TPB can vary with thickness. Since deposition occurred after the AV was fully populated with PMTs, an optical flasher circuit using LEDs mounted on the TPB source itself was developed for operation during the deposition. It was hoped to gain real-time information on the growth of the TPB layer, and with the addition of other optical calibration sources, generate an overall TPB thickness map.

Visible photons that are absorbed in the TPB layer will be re-emitted with a re-emission time around 1 ns. As the thickness of the coating increases, the chance for multiple scatters increases. For sufficiently fast incident light pulses, the net effect is a decrease in the number of first-arriving photons at each PMT before the collection of subsequently scattered photons inside the rest of the detector. This attenuation in first-arriving photons can be used as a relative channel by channel mapping of the TPB coating. Additionally, any impurities in the TPB can lead to absorption of re-emitted light, which can increase with a thicker applied coating.

A fast light pulser, as described in [32] was built using C503B-BCN-CV0Z0461

High Brightness LEDs. The DEAP-3600 detector is approximately 1.5 m in diameter, or approximately 4 ns across. Because the AV shell is covered in a diffuse reflector to prevent the complete loss of light not initially incident on a light guide face, the light pulses from these LEDs must be sufficiently fast to produce a clean signal before reflections. Measurement of the coating thickness can be taken from those first-arriving photons as opposed to late photons from reflections about the AV.

The difficulty in creating fast flashes comes not from charging the LEDs, but from slow current leaking out of the device after being switched off. That is, the total width of the light pulse is driven by the decay time, rather than the rise time. To shorten this width, current is driven in the opposite direction through the LED, forcing a fast switch-off. This pulser was operated with a -2.5 V square wave trigger superimposed on a 0-30 V negative bias.

The initial version of this circuit that was built did not produce pulses with the fast timing characteristics expected. It was suspected that some components used may have been faulty. Additionally, the type of LED being used may have been an issue [33]; not all stock LEDs can be driven at the speeds required. A pulser of similar design was provided by L. Thompson that was developed for the ANTARES experiment [34]. This circuit, shown schematically in Figure 3.4, was modified to drive 2 LEDs. The LEDs were placed in parallel to develop the same timing output.

Mounting many LEDs on the TPB source, and driving them at the same time, was not feasible. Even with an opening angle of 100 degrees, full LED coverage at the AV inner surface could only be achieved with a minimum of 12 LEDs. Diffusing the LEDs by lightly sanding the surface of the epoxy potting can greatly increased opening angle, at the expense of individual light output uniformity. With this, the

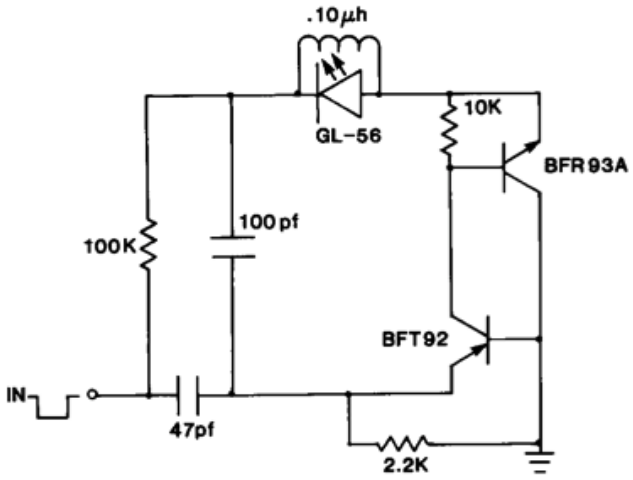

Figure 3.4: The LED pulser used in the development of the TPB source mounted flasher was based on the design in [32].

number of LEDs required to illuminate the entire AV can be reduced to two. As long as the source position does not change during data taking, a difference measurement pre- and post-deposition will correct for the non-uniformity in the light output from the LEDs.

Results from in situ TPB thickness measurements on the test vessel at Queen's are found in Chapter 5. Prior to deployment in the vessel, the LEDs mounted on the TPB source were abandoned due to difficulty in mounting, cooling, and risk to the detector.

3.4 Coating Specifications

Specifications as to the TPB deposition outlined in [35] are listed below:

- Coverage over entire inner AV surface: no pinholes or uncoated areas

- Detector neck should not be coated in TPB: this could lead to background neck

events or potentially flake off during insertion of the acrylic flow guide

- Coating should be stable over lifetime of the experiment
- Source to be used (empty) for vacuum bake of the vessel post resurfacing
- Source and deployment system should adhere to radio-purity requirements: 10 mBq radon emanation limit
- Source position to be known to better than 1 cm

Additionally, fluctuations in coating thickness were to be kept under 20% across the detector. Prior to deposition, a vacuum bakeout was performed on the acrylic vessel to remove water absorbed into the surface from post-resurfacer flushing. Residual water vapour diffusing out of the acrylic surface has a negative effect on TPB coating quality, and can lead to quenching of the argon scintillation signal [36].

The thickness of the TPB coating for DEAP-1 varied from 1-4 micrometers depending on the generation [37], but was thinner on the windows than on the chamber body. Although complete coverage is most important to convert the VUV light from argon scintillation into the visible region, a thicker TPB layer additionally helps in surface background mitigation. Po will at some level be present on the acrylic surface or in/on the TPB layer. For Po decays between the argon and TPB interface, half will send alphas into the TPB layer. Increasing the thickness of the TPB layer through which this alpha travels increases the amount of scintillation and can be used to effectively boost the Po decay out of the energy region of interest (ROI) between 15-30 keVee.

As a brief estimate, 100 keV nuclear recoil is quenched to 25 keVee [36]. To boost the signal above the 30 keVee ROI bound, an additional 5 keVee must be generated

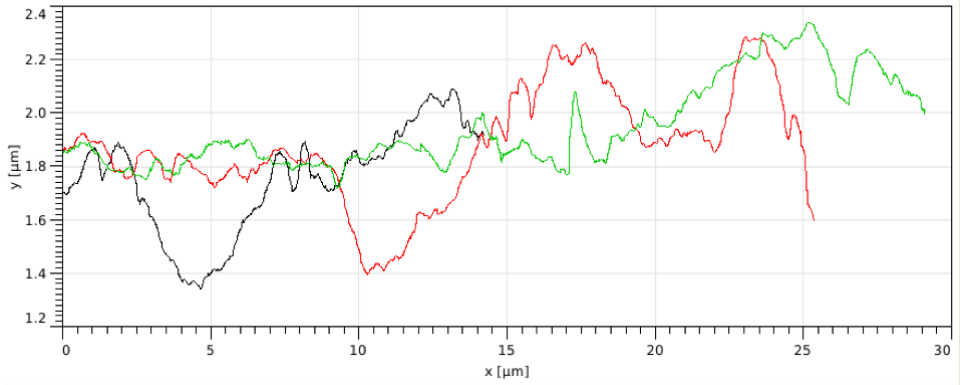

Figure 3.5: AFM scan showing surface roughness of sanded acrylic. The three colors represent different contour lines.

in the TPB layer. With a nominal light yield of 8 PE/keVee expected for DEAP-3600, this corresponds to an additional 40 photons. TPB, under alpha scintillation, produces roughly 882 photons/MeV [24]. Assuming a 20% detection efficiency, these photons would leave around 226 keV in the TPB layer. With an approximate 160 keV/µm stopping power, the TPB layer would need to be 1.4 microns thick to boost this recoil event.

The ultimate consideration for the thickness of the coating comes from the complete coverage requirement. Figure 3.5 shows an atomic force microscopy (AFM) scan of a test piece of acrylic sanded with the same sanding paper as used on the resurfacer. Surface roughness features range from 1-2 micrometers. To ensure complete coverage of the acrylic surface, the TPB coating must be thick enough to jacket these underlying surface features.

Chapter 4

Source Deployment System

The goal of the deployment system is to allow clean entry for sources inside the detector prior to filling with argon. Access into the AV begins through the glovebox at the top of the neck which is continually purged with radon-scrubbed boil-off nitrogen. It is in the glovebox that source manipulation and insertion occurs, after which the sources must traverse the length of the 3 meter neck before entering the AV. Initially the system was designed to be compatible with both the TPB deposition system and the two optical calibration sources: a 405 nm laser ball and a UV LED ball. As calibration and TPB deposition are done after resurfacing of the AV, all components of the deployment system must undergo a radio-purity assay program. Work on the initial design, as well as the final deployment system design is presented.

4.1 Initial Design

The initial concept of the deployment system was outlined and designed by S. Florian and M. Kuźniak. Entrance into the AV starts on the deck, inside the glovebox. Here, shown in Figure 4.1, a vacuum-sealed deployment cross is attached to the top of the neck. A custom 10" CF 5-way cross mating to the 12" CF neck flange

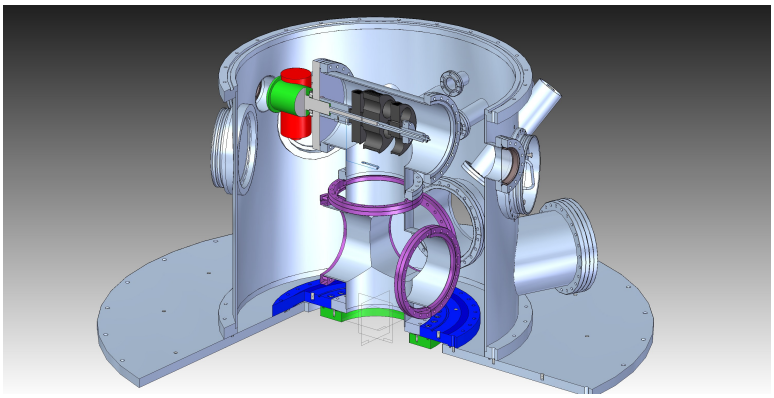

Figure 4.1: Conceptual drawing of the initial source deployment system.

would provide a path to the vacuum pump out port. Access into the AV would be provided with a vacuum feedthrough motor and shaft assembly, and the sources would be unrolled off a cable bundle. All signal and power cables would be routed through vacuum feedthroughs after being rotationally decoupled with a slip ring. The following sections cover the main components of the initial design, as well as the final deployed design.

4.1.1 Motor

Sources could be lowered into the AV by a motor mounted to the deployment tee inside the glovebox. A McLennan Sim-step drive motor was mounted to a 10" CF flange with 2.75" zero length reducer. The motor could be controlled manually via a jog box, or through RS232 connection to a computer running McTerminal, the software provided by McLennan. The limit switches attached to the motor were removed to allow continuous (unbounded) raising and lowering of the source. An encoder on the motor allowed for the number of steps to be read out. A stainless steel shaft extension coupled to the existing motor shaft on the vacuum side of the 10" CF flange. The

motor itself was outside the vacuum space and not subject to as strict radio-purity requirements, as it would sit in a nitrogen purged environment inside the glovebox.

4.1.2 Bobbins

The sources, hanging off the deployment cable, would be lowered into the detector by being unrolled off a series of bobbins. Three custom bobbins were created from high density polyethylene; one for the main signal cable bundle, and two side units for stability and additional stage hanging and signal readout. These bobbins were designed to allow deployment of both the source and stage simultaneously. They were tuned such that the stage would come to rest at the neck-sphere interface of the AV while the source would be positioned in the center of the detector. A 3.5 mm pitch was created in the main bobbin, which placed constraints on the size of the main cable bundle. The pitch of the two side bobbins was set at 1.2 mm, or the diameter of one 50HCX-18 coax cable. The bobbins included a pitch to assist in winding and unwinding the cables consistently. This would allow the cables to track side-to-side on the bobbin and prevent the cable from winding onto itself. Keeping a constant length of cable per wind on the bobbin (that is, a constant bend radius) is necessary for accurately determining the source position in the AV.

4.1.3 Laser distance gauge

A Micro-Epsilon optoNCDT ILR 1181 laser distance gauge was tested for checking the final position of the source. Space constraints inside the deployment system and vacuum compatibility required that the distance gauge be placed outside the vacuum space. Using a series of mirrors and a 2.75" CF vacuum compatible window, the

beam from the distance gauge could be projected into the deployment tee and down the neck to the source. Small pieces of specular reflector were cut and positioned in the deployment tee out of reach of the bobbins to reflect the outgoing and incoming beam lines. A stainless steel mounting plate for the laser gauge was built that affixed to the 2.75" CF window. The beam from the laser would be reflected once at 90° to enter the deployment tube, then again by approximately 90° to traverse the length of the neck into the detector.

Distance tracking could be commanded via the RS232 connection. As an initial line-of-sight test, the TPB source was lowered in the test setup at Queen's, Figure 5.1, and its distance monitored. In this test, the beam and source were inline. Logging accuracy of the distance gauge was to the nearest millimeter, although the gauge can be set to a 0.1 mm resolution. Knowledge of the source positioning to better than 1 cm is outlined in the TPB specifications document [35]. The distance correlated with the number of steps the motor had taken can be seen in Figure 4.2. The equation relating number of steps to physical distance was calculated from a linear fit to be:

$$distance[m] = 1.411 \times 10^{-5}(n_{step}) + 0.612 \tag{4.1}$$

Using 4.1, for a final source position in the DEAP-3600 AV of 2.57 m from the resting position in the deployment tee, the number of motor steps required to lower the center of the source to the center of the detector is 138766.

4.1.4 Cable Bundle

Sources would be attached to a cable bundle which in addition to support, carries the electrical connections. Two cable bundles, one 4 meter prototype and one 6.5 meter

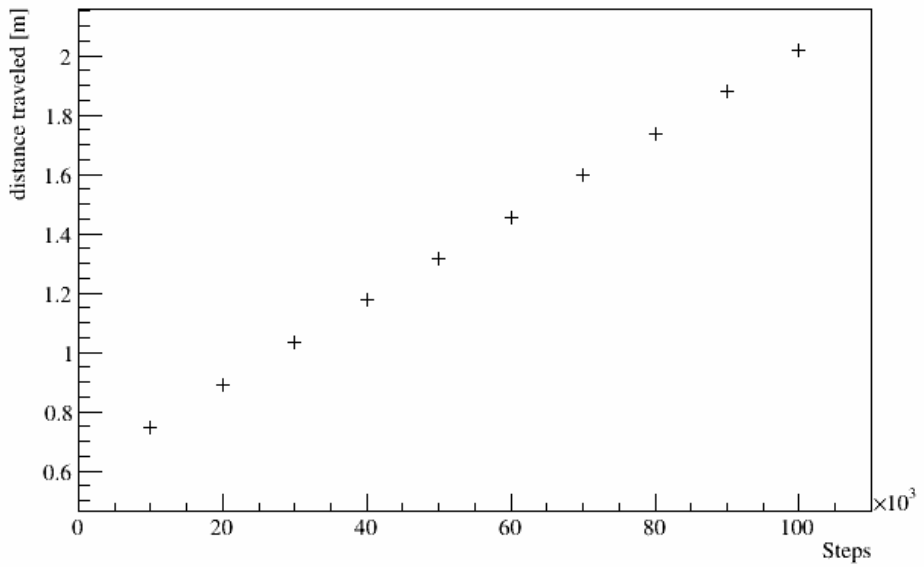

Figure 4.2: Number of motor steps plotted against recorded distance traveled using Micro-Epsilon laser gauge during a test run.

production, were created. The individual cables inside the bundle and their functions are listed in 4.1. The cables were bound in 1 foot sections of un-shrunk Fluorinated Ethylene Propylene (FEP) heat shrink to keep them together and within the 3.5 mm pitch of the bobbins. Initially, small bands of FEP heat shrink were spaced at 1 foot increments, but the splaying of individual cables proved to cause winding problems. Encapsulation in sections would allow the cables to be individually cleaned once, then further cleaning would require only wiping the outer casing.

The 4 meter cable was used for initial testing of the deployment system in the vacuum system at Queen's. The final production cable measured 6.5 meters to allow access not only to the center of the detector for the TPB source, but allow additional movement above and below center for the calibration sources. Proposals from the

quantity	cable	core	usage
1	stainless steel	braided	structural
2	line voltage cable	solid	power
2	Lakeshore Cryogenic Wire	4 solid core	temperature readout
1	50HCX-18	coaxial	triggering

Table 4.1: Specifications for the prototype and production cable bundles.

calibration group for optical source positioning were to take data in the center of the detector and 2 additional symmetric positions in the z-axis, which co-aligns with the center of the detector neck.

The construction for both cable bundles was similarly performed. Each individual cable was measured, cut for length, and wiped cleaned with ultra pure water (UPW) and isopropyl alcohol (IPA), then laid out on a cleaned lab counter top and shielded from room dust with a thin plastic tent. One foot sections of the FEP heat shrink were cut, then rinsed with UPW and IPA. One end of each cable in the bundle was fixed in place with gaffer tape. All six cables were threaded into the tubing at the same time, with care to keep the relative positioning of each cable constant (no twisting). The leading loose cables were continually wiped down before the newest FEP tubing was slid over. Each section of tubing was incrementally progressed down the cables, keeping as much of the cable protected from room dust and preventing as much twisting of cables inside the tubing as possible. The process was repeated until the entire length of cable was bound in FEP, leaving one foot of loose cable at the top end for electrical connections. The final cable bundle was wiped with UPW and gathered loosely into a coil and bagged before being wound on the main cable bobbin. Figure 4.3 shows the cable bundle on the main cable bobbin.

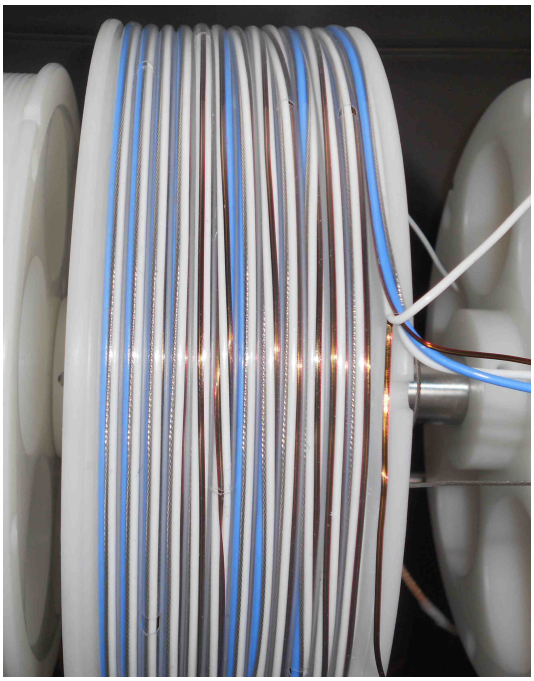

Figure 4.3: Cable bundle, with the cables listed in Table 4.1 on the main bobbin.

4.1.5 Slip ring

All electrical connections through the vacuum space are static. Because the sources would be unrolled from the bobbins on the motor shaft, it was necessary that all power and signal cables be connected with rotary slip rings. A Fabricast 09814 14-wire slip ring for instrumentation (power, temperature, and control) and a JINPAT LPCC-01 coax slip ring (signal) were installed. Space constraints set a limit of only one coax slip ring, requiring additionally a Ducommun TOH series miniature SPDT radio-frequency switch for channel multiplexing to remotely switch between the two coaxial readout channels proposed during TPB deposition: deposition monitor readout and LED triggering on the TPB source. A LabView controlled relay could switch between the readout channels. Figure 4.4 shows a picture of the slip ring on the shaft extension, with bobbins attached.

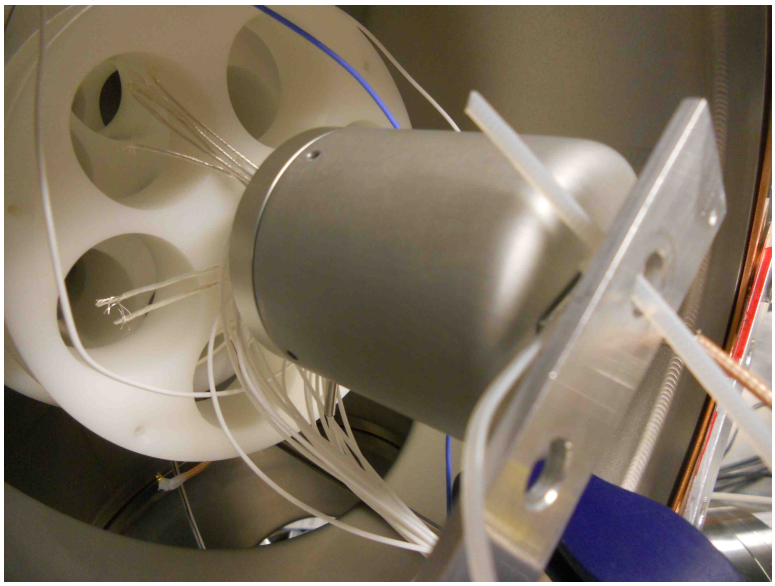

Figure 4.4: View inside the deployment cross of the 14-wire slip ring and secondary bobbin.

4.1.6 Stage

A multi-purpose stage was developed to be deployed at the intersection where the acrylic neck joins the acrylic sphere. The main purpose of this platform is to serve as a baffle to prevent extraneous TPB coating up the neck. The TPB source emits molecules isotropically, and there is a solid angle viewed by the source that sees directly up the neck. Excess or unintentional coating of the neck with TPB could lead to light being generated outside the AV spherical volume leaking into the vessel. Additionally, TPB may flake off the neck when the final argon flow guides are installed. A full list of functions for the stage is given in Table 4.2.

For TPB deposition, the desired pressure in the AV was below 1×10^{-5} mbar to ensure the molecules emitted from the source travel directly to the inner surface of the AV without scattering en route. The effectiveness of the stage baffle is decreased when the impinging TPB is not ballistically deposited (i.e. if the impinging molecule

Form	Function
Baffle	Prevent excess coating of TPB in neck
Mounting for quartz deposition monitor	Direct measurement of the TPB coating thickness at the radius of the AV
Mounting for infrared temperature sensor	Measure inner acrylic surface temperature during AV bake-out and TPB deposition
Mounting for additional RTD sensor	Redundancy in acrylic temperature measurement
Target for distance gauge	Accurate positioning of the stage is needed to prevent coating of the neck
Stability	The two side bobbins keep the stage in a fixed position. From the stage, an additional set of cables can be extended to keep all sources rotationally stable.

Table 4.2: Uses of the multi-function stage deployed in the intersection of the acrylic neck and spherical volume.

trajectory does not point directly back to the source). To achieve this, the baffle must not completely cut off the flow path from the spherical AV through the neck; conduction must be maintained to allow adequate molecular flow during pumping. However, it must cover the visible solid angle from the TPB source to catch neck-bound molecules. A skirt, made from Tyvek (Figure 4.9), was attached to the stage, schematically shown in Figure 4.5, to allow coverage, yet adequate conduction from the AV.

4.2 Final Design

Despite the development of the initial deployment system, several major issues were left outstanding as resurfacing was beginning (immediately preceding TPB deposition in the construction schedule):

Cable straightness

Constraints from the pitch of the bobbins required the cable bundle be 3.5 mm in diameter. To allow for all signal and power cables to be bound together, the cables needed to lay parallel in the FEP casing; the individual wires could not be braided with respect to each other. The latter treatment is typically used to keep loosely bound cables together when bending around a radius, like that of the bobbins. Giving the individual wires a twist allows relative motion between cables. With the individual cables laying in parallel, each cable in a bundle will have a slightly different bend radius. With a fixed length for each component cable, this caused the individual ends to become increasingly separated as the cables were wound and unwound. Tension and friction inside the bundle created kinks during unwinding, typically in the thermocouple and coax cables as they were more flexible. As the cable was unwound, these kinks proved to not straighten out under the weight of the hanging sources. Upon re-winding, this would often lead to skipping of threads on the bobbin, and in several severe cases caused the wire to fall off the bobbin completely. If this were to happen in the final setup in the deployment tee, it would not be seen and not easily, if at all, correctable in situ. Reproducibility in final positioning would become non-linear with respect to the steps-per-distance in Figure 4.2, as there would be some vertical offset taken up by the kinked cable.

Cable Bundle Cleanliness

Although the individual cables were cleaned prior to threading through the FEP encasement, during the course of testing dust and particulates became trapped inside the casing as it became statically charged and over-handled. Furthermore, the end faces of the FEP tubing became increasingly flared. This was caused by the edges of the tubing catching on the cable guide which centered the bundle in the neck. Although this never resulted in the cable catching or excessive torque on the motor, it did become increasingly noticeable. In the lower section of the cable, an area of increased friction between neighboring sections of FEP tubing was noticed where one section began sliding over the other.

Installation complexity

Space, and visibility of said space, inside the glovebox is very limited, and physical access is only available through 6 glove ports. Although the deployment tee and 5-way cross were designed to fit inside the glovebox, they would not fit through the gate valve on the top of the glovebox together. Figure 4.1 shows a conceptual sketch of the deployment system inside the glovebox. Additionally, their installation once inside the purged glovebox was highly non-trivial. All 10" CF and 12" CF flanges would need to be sealed through the glove ports. An outline of the more complex installation tasks follows:

- Deployment tee and 5-way cross installation: work attaching the 12" CF and 10" CF connections from the neck to the 5-way cross, and then to the vacuum pump out port must be done in a sealed, nitrogen-purged environment.
- Source installation: Changing of the source (TPB/heater or optical) must be

done in a purged environment. Each source change is accompanied by the re-sealing of the 10" CF deployment tee access port. Great care must be given as work inside the deployment tee exposes the entire length of the neck and AV to dropping loose tools or bolts.

- Source orientation: Installing the source inside the neck means working with the sources with the AV exposed. The orientation of the TPB/heater source is not important once fixed into position. However, orientation of the optical calibration sources must be understood in order to deconvolve the non-uniformity in light distribution from the source to that of the actual detector optical response. Data, taken at varying phi-rotations of the calibration source, could be used to understand the source non-uniformity. To accomplish this with the initial deployment scheme, the source would need to be raised out of the AV and deployment tee, rotated, then re-attached and replaced for each phi rotation.

- Removal of the deployment system: once the TPB deposition and optical calibration has taken place, the entire system must be cleanly removed to allow access for the cooling coil installation. Again, all bolts must be loosened through the glove ports and maintained in a nitrogen-purged environment.

In lieu of these outstanding challenges, the author proposed a simplified re-design of the deployment system. Utilizing the deployment canister for the resurfacer, a semi-rigid pipe would be lowered into the AV instead of a cable. This new system would allow the same functionality of the initial system (source connections, z-position adjustment) but with no rotating parts. Additionally, many of the constraints from the initial design (space, connection limitability, source rotation/stability) were directly

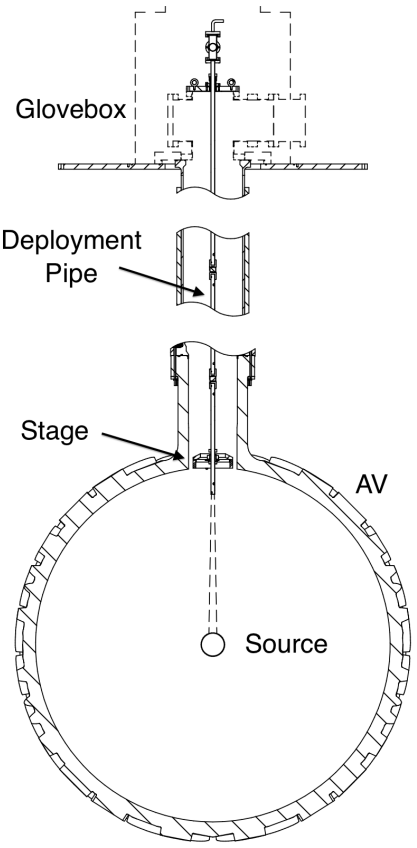

Figure 4.5: Schematic of the DEAP-3600 detector, glovebox, and deployment canister with the final deployment system. The deployment pipe can be retracted into the canister on top of the glovebox. All volumes can be purged before its installation in the AV.

resolved. All internal structural components of the deployment system were made of stainless steel, except the electrical cables and vacuum feedthroughs. An overall schematic of the deployment system can be seen in Figure 4.5 and Figure 4.6.

4.2.1 Deployment Pipe

Access into the AV via a motor and bobbin assembly was replaced with a fixed length stainless steel 0.75" diameter pipe articulated in two places using stainless steel

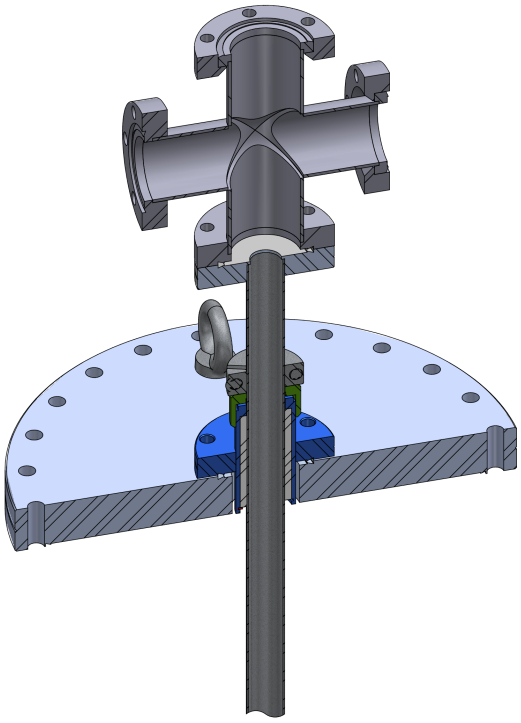

Figure 4.6: Conceptual sketch of the deployment system top cross. Power and signal cables connect through the top cross, as well as a nitrogen purge line. The vacuum seal is made through the Quick Disconnect flange (blue) sealing the top 10" CF flange to the deployment pipe.

universal joints. A solid 18 foot stainless pipe would inherently have some deviations from being straight over the length of the pipe. Because source positioning should be known to centimeter resolution, both in z- and radial-position, the length of the pipe was sectioned and joined with universal joints; the deviation in straightness over the length of 6 feet should be minimal.

The cables hang loosely inside the 0.75" stainless pipe and are routed outside the

pipe to get around the universal joints. The necessary cables were migrated from the initial cable bundle design. Each cable was removed from the FEP tubing, checked for electrical conductivity, cleaned with UPW and IPA, then bagged. The 50HCX-18 coaxial cable was also checked for continuity and transmission of signal.

The top of the deployment tube was vacuum sealed to the existing 10" CF motor flange with zero length reducing 2.75" CF center bore. The seal comes through a commercially available 2.75" CF to 0.75" Quick-Disconnect adapter, which is designed to mate from ConFlat sealing surfaces to generic 0.75" outer diameter pipe. A threaded cap compresses an O-ring which seals to the 0.75" pipe. The O-ring seal was tested to a better vacuum than required for the TPB deposition: $\mathcal{O}(5 \times 10^{-7})$ mbar. It was found that the stainless on stainless contact from the 0.75" pipe and inner bore of the Quick-Disconnect flange was causing scratching on both surfaces. A custom Quick-Disconnect flange, based on the stock design, was created with an acrylic insert sleeve. This makes changing the z-position of the deployment pipe easier, and resolved the binding from the stainless on stainless contact.

All electrical connections were brought out of the vacuum space through a 4-way 2.75" CF tee on the top of the deployment pipe. A Pasternack PE44353 RG174 coax connector to BNC flange and one 19 pin signal and power feedthrough flange were mounted to a 4-way tee. A nitrogen purge line input was installed which connected to an 0.25" FEP tube routed in the deployment pipe and allowed purging of the detector volume during installation. The final assembled top cross for the deployment system is shown in Figure 4.7.

The requirements for the stage remained the same as from the original design. Three acrylic sample slides, 2 inches in diameter were affixed to the bottom of the

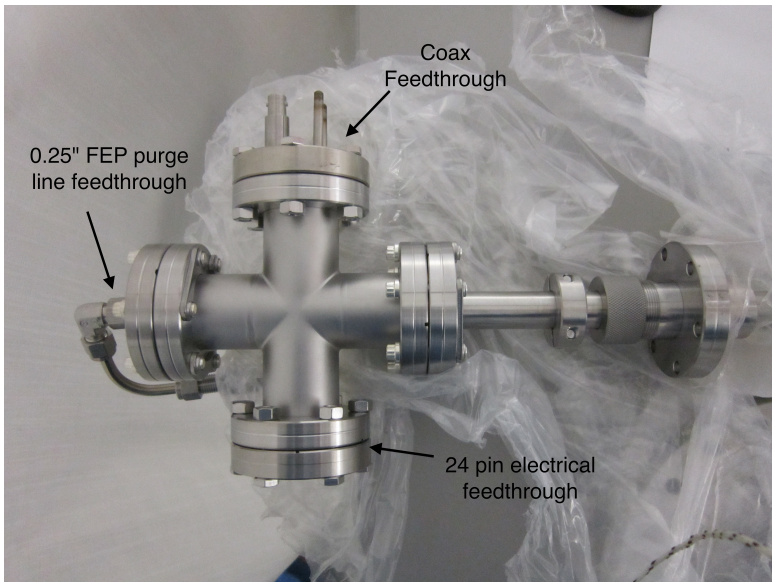

Figure 4.7: Final assembly of top cross for the deployment pipe.

stage. Two of these samples were sanded to a surface finish similar to what is expected from the resurfacer. The third sample was left with a polished, un-sanded finish. These samples were removed after the TPB deposition to examine and characterize the coating ex situ. The Omega OS36 infrared probe was mounted, along with the Inficon quartz deposition monitor. A top cone was installed to act as a guide when retracting the deployment system from the AV. There is a clearance of 0.25" between the outer diameter of the stage and inner diameter on the bottom orifice of the 5-way cross. If the stage were off centered during retraction, it could potentially catch on the inner diameter.

To block TPB from entering the neck, a three part Tyvek skirt was attached to the stage. A sectioned schematic is shown in Figure 4.8. One piece, held to the bottom of the stage, covered the gap between the outer diameter of the stage to the inner radius of the acrylic neck in the AV, while was open in the center. A second, complimentary top skirt blocked the center opening from bottom stage skirt. A third Tyvek piece was

wrapped coaxially along the outer stage diameter to block any remaining visible solid angle from the source to the neck. The complexity of the baffle was brought on by requiring complete solid angle coverage, while still providing adequate conduction for the vacuum. The final stage assembly, before and after Tyvek skirting was installed, can be seen in Figure 4.9.

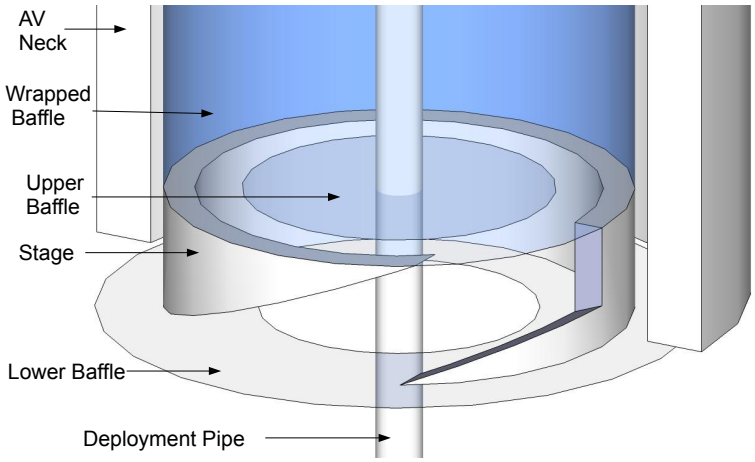

Figure 4.8: Sectioned schematic view of the baffle on the stage. Two baffles, an upper solid circular and lower complimentary ring cover the visible solid angle viewed from the source, with an additional coaxially-wrapped piece.

4.2.2 Cleaning

All small metal components of the deployment system were ultrasonically cleaned with Alconox and UPW. The sections of pipe were scrubbed with Alconox and UPW on the outside and cleaned internally by flowing hot UPW through after an initial pass with Kimwipes soaked in Alconox. Additionally, the Quick-Disconnect and welded 2.75" CF flange end of the top section of the deployment pipe were citric acid passivated

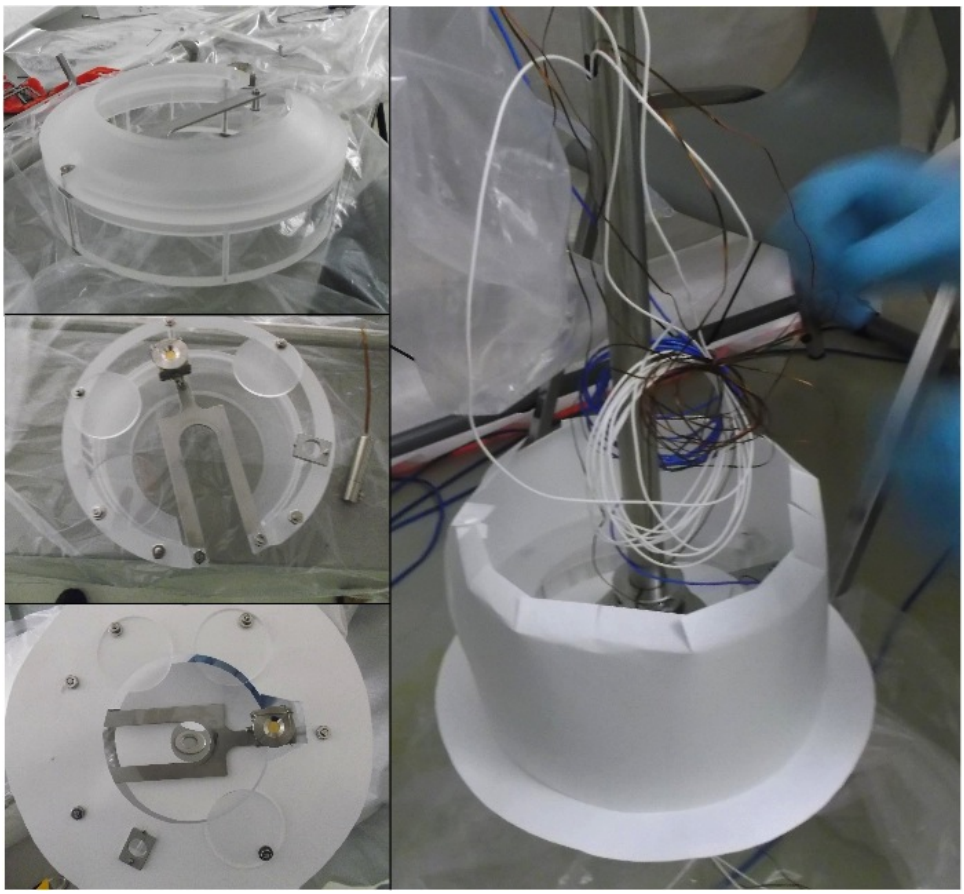

Figure 4.9: Counter clockwise from top. Top: Acrylic stage with alignment cone. Middle: Underside of stage (AV side) with acrylic samples, deposition monitor visible. Bottom: Underside of stage with Tyvek skirt installed. Acrylic samples, deposition monitor, and mount for IR probe still visible. Right: Stage with Tyvek baffle completed. Excess electrical wires tied up above stage for transportation from the Cryopit to the Cube Hall for installation.

and rinsed with UPW.

Chapter 5

Systems Testing

Initial testing of the prototype source was carried out by T. Pollmann [27]. In these tests, TPB coatings were sampled at discrete points from the source at the radius of the DEAP-3600 acrylic vessel (85 cm). The same vacuum system used in these initial tests was rebuilt to allow for the installation of a 20 inch test vessel and further testing of the deposition and deployment systems. Though a smaller volume than the DEAP-3600 AV, the test vessel includes 6 full sized light guide stubs. A 2 meter 10" CF neck was constructed to connect the vessel to a 1250 l/s Pfeiffer turbomolecular pump (TMP) with a Pfeiffer XtraDry roughing pump. The re-built vacuum system can be seen in Figure 5.1.

5.1 Bakeout testing

To prevent TPB molecules leaving the source from scattering on route to the inner surface of the detector, a mean free path greater than 0.85 meters is desired. As discussed in Chapter 4, preventing scattering from the source to the inner surface is needed to keep the effectiveness of the neck baffle in preventing coating up the neck. Additionally, if the pressure in the AV is too high and the molecules collide before

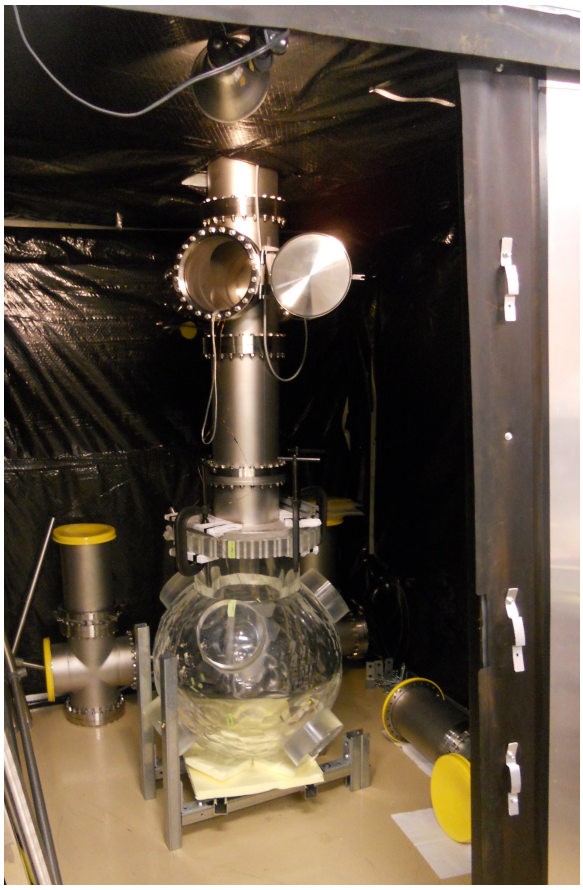

Figure 5.1: 20 inch test vessel setup at Queen's inside the dark box.

reaching the surface of the AV, they will cool, further driving down their mean free path.

To prevent scattering, through application of Equation 3.2, an initial pressure better than 1×10^{-5} mbar is necessary inside the AV. Because the AV was continually rinsed with UPW during resurfacing, the acrylic became saturated. Water which soaked into the acrylic will outgas under vacuum making the required pressure difficult to achieve in a timely manner. Heating the inner acrylic surface mobilizes adhered and diffused in molecules. Performing this baking under vacuum allows these molecules to be evacuated from the volume by use of the TMP. Using the TPB deposition

source empty, that is purely as a heating source, the inner surface of the DEAP-3600 acrylic vessel was heated to near 50°C, discussed further in Chapter 6. The maximum temperature for the annealing of the DEAP-3600 vessel was 85°C, and care was taken to keep a controlled temperature gradient during heating and cooling [38]. For the AV bakeout, the following temperature constraints were placed [39]:

Source Temperature: not to exceed 205°C

Inner AV Surface Temperature: not to exceed 50°C

Temperature Gradient: less than 10°C across AV wall thickness

The heating element on the TPB source provides 275 watts heating power. Early heating tests showed the inner surface of the test vessel could be brought to a temperature of 60°C in about an hour. It was estimated this would translate to around 10 hours of heating to get the DEAP-3600 AV inner surface to temperature (this comes from the nearly factor of 10 increase in AV inner surface area from the test vessel to the full scale vessel). However, finite element analyses done by C. Ng indicate that it would take 3 days to raise the temperature of the inner surface to 50°C [39]. The difference in estimated heating time comes from the competing process pulling heat out from the inner surface towards the outer AV and steel shell. Final bakeout results are presented in Chapter 6.

The goal of the first bake out on the test vessel was simply to see if the inner surface of the detector could be brought to a temperature of 60°C on the hour timescale. The modified prototype TPB source was deployed empty in the test vessel and run at full power while an RTD affixed to the inner surface of the acrylic with Kapton tape was monitored. The temperature as a function of time can be seen in Figure 5.2.

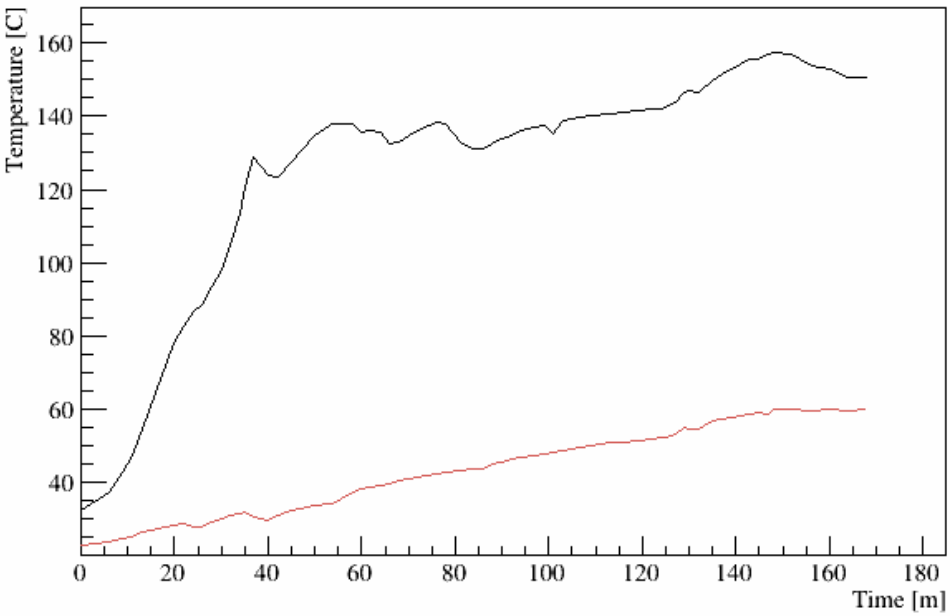

Figure 5.2: Heating test 1 profile. Red: AV temperature. Black: source temperature

Once the functionality of the TPB source as a heater was confirmed, a Pfeiffer PrismaPlus residual gas analyser (RGA) was used to monitor the outgassing during bake-out. Code written by M. Ward was used to analyze the data. Ion current, which is proportional to particle count, as a function of atomic mass is fit with the individual fragmentation patterns available from NIST for various expected molecular species. The outgassing spectra were continually gathered over the period of the bake-out. The heating profile of the source and inner surface temperature for this test can be seen in Figure 5.3.

An example spectrum recorded by the RGA can be seen in Figure 5.4. Here, the black curve represents the spectrum of the test vessel while at 23°C as recorded by a

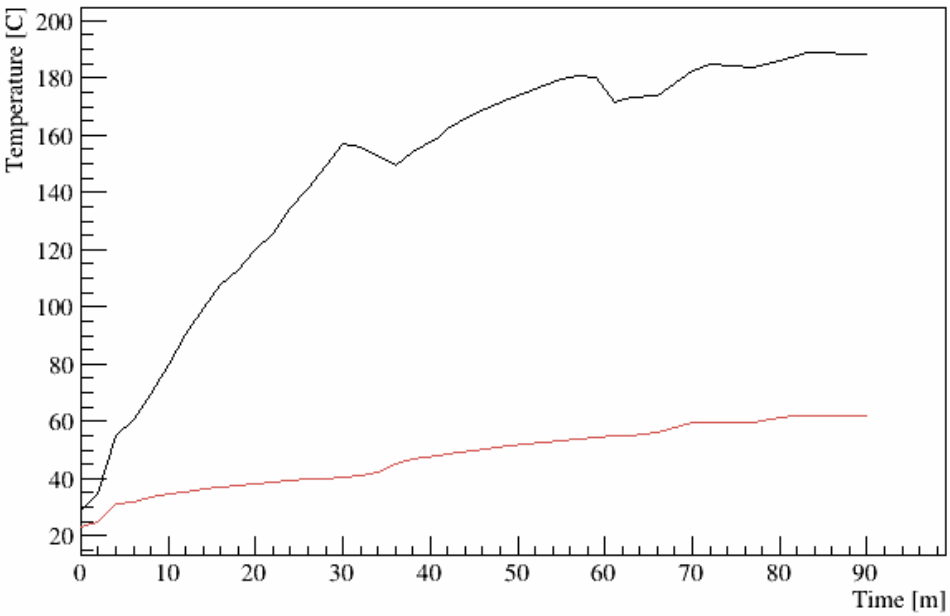

Figure 5.3: Heating test 2 profile. Red: AV temperature. Black: source temperature

RTD placed on the inner surface of the acrylic. The red curve is the RGA spectrum when the inner acrylic temperature was raised to 60°C. It can be seen that the overall pressure increases as the temperature of the acrylic increases, which is the result of the higher outgassing rate from warm acrylic.

Additionally from Figure 5.4, the largest contribution to the outgassing rate is from water (AMU 18). The overall RGA spectrum can be fitted for the spectra of individual species to find the partial pressure of each. The fitted percent abundances for the two spectra in Figure 5.4 are shown in Table 5.1. The total percentage in each is calculated to be over 100%, however this is known artifact of the analysis code.

In the third of the initial heating tests, the inner surface of the AV was again

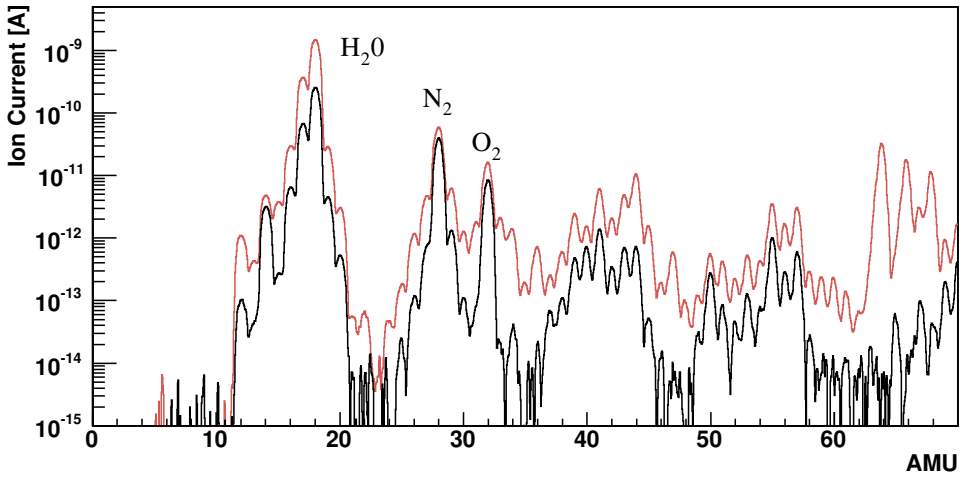

Figure 5.4: Comparison of RGA spectra during vacuum bakeout. Red is at 60°C and black is at 23°C before baking.

brought to a temperature of 60°C, albeit more aggressively than the prior runs. Using the throughput method for measuring outgassing rates, the test vessel was continually pumped on with the TMP while the inner surface was brought to temperature. Knowing the conduction C of a system and the surface area A outgassing, the outgassing rate is calculated as [40]:

$$Q = (P - P_0) * \frac{C}{A} \tag{5.1}$$

The conduction calculation for the test vessel setup was calculated following [41]. The turbo pump was connected to the vessel through a section of 10" CF full nipples 0.85 m long, followed by a 90 degree bend, then an additional 0.94 m 10" CF full nipple section. The 90° bend, in the region of molecular flow, is equal to the conduction of a straight section of pipe with length equal to the arc distance in the bend.

Spectrum	Component	Abundance
22.98°	water	90.0456
	nitrogen	6.88041
	carbon monoxide	2.99407
	isopropyl alcohol	2.47101
	oxygen	2.35679
	ammonia	1.53185
	argon	0.150616
	neon	0.0854144
	carbon dioxide	0.0844691
	methane	0.0408901
	total	106.641
60.09°	water	96.0671
	isopropyl alcohol	2.85119
	nitrogen	1.78367
	ammonia	1.4792
	carbon monoxide	0.999543
	oxygen	0.848618
	carbon dioxide	0.316079
	neon	0.131935
	argon	0.0943051
	methane	0.0909454
	total	104.663

Table 5.1: Results from fitting fraction patterns to the RGA spectrum. Individual components (partial pressures) are broken down from the total spectrum.

The conduction in the test setup, which is a measure of the flow in a system, is calculated from:

$$\frac{1}{C_{total}} = \frac{1}{C_1} + \frac{1}{C_2} + \frac{1}{C_3} \tag{5.2}$$

where C_i represents the conduction through pipe i in the test setup:

$$C_i = \frac{d^3\pi}{12l}\bar{c} \tag{5.3}$$

where d is the diameter of the pipe, l the length, and $\bar{c}$ is the mean thermal speed of air at 20°C which has the value of 464 m/s. The total conduction C_{total}, for the test setup with $C_1 = 1.2$ m^3/s, $C_2 = 2.68$ m^3/s, $C_3 = 1.08$ m^3/s is then equal to 469 l/s. With the rated pumping speed of the TMP being 1250 l/s, the gas load in the system can be calculated as:

$$Q = P * S_{eff} \tag{5.4}$$

for P the final attainable pressure in the vessel, and S_{eff} the effective pumping speed at the chamber. The final attainable pressure in the vessel was 9.45×10^{-6} mbar and $S_{eff} = 341$ l/s. This leads to a gas load in the test setup of:

$$Q_{exp} = 3.22 \times 10^{-3} \text{ mbar l/s} \tag{5.5}$$

The listed de-absorption rate for acrylic is 4×10^{-7} mbar l/s cm^2 [41], which leads to a theoretical gas load:

$$Q_{theory} = 3.24 \times 10^{-3} \text{ mbar l/s} \tag{5.6}$$

These two values, Equations 5.5 and 5.6, are in good agreement (0.6% error) given the simplifications in system dimensions for the conduction calculation, and the assumption that the stainless steel vacuum system had a negligible contribution to the overall gas load.

Additional heating tests were performed with increased instrumentation. These tests were to understand better the heating profile and power input into the vessel during baking, as well as to exercise the readout and control electronics. RTD sensors

were placed on the interior and exterior of the test vessel shell along the same radial axis. Data from the infrared sensor was also logged along with the heating source. Figure 5.5 shows the result of this test.

The intermittent breaks in the data logging are the result of losses in power of the entire system. When this happens, the Lakeshore temperature controller is latched off and power is shut to the system. It is seen that when power is restored and infrared radiation is being emitted from the source, the inner AV surface temperature quickly rises. Latching off the power to the heater was necessary as the test was performed overnight when there was no direct supervision of the system. For this test, the RTD sensor taped to the inner surface of the AV was set to trip the power relay in an effort not to over heat the acrylic.

The source temperature, in black, decreases as the acrylic temperature rises. Once the bulk acrylic starts to come to temperature, less input power is required to maintain an elevated inner surface temperature, and the duty cycle of the heater running at full power is reduced. Also seen on the plot is the lag between the inner and outer surface temperatures of the acrylic shell. Correlating the inner surface RTD measurement with the infrared temperature probe (blue) shows the lag in time from the heating of the immediate surface to bulk heating; the IR temperature sensor probes into the acrylic a few millimeters, rather than just the surface.

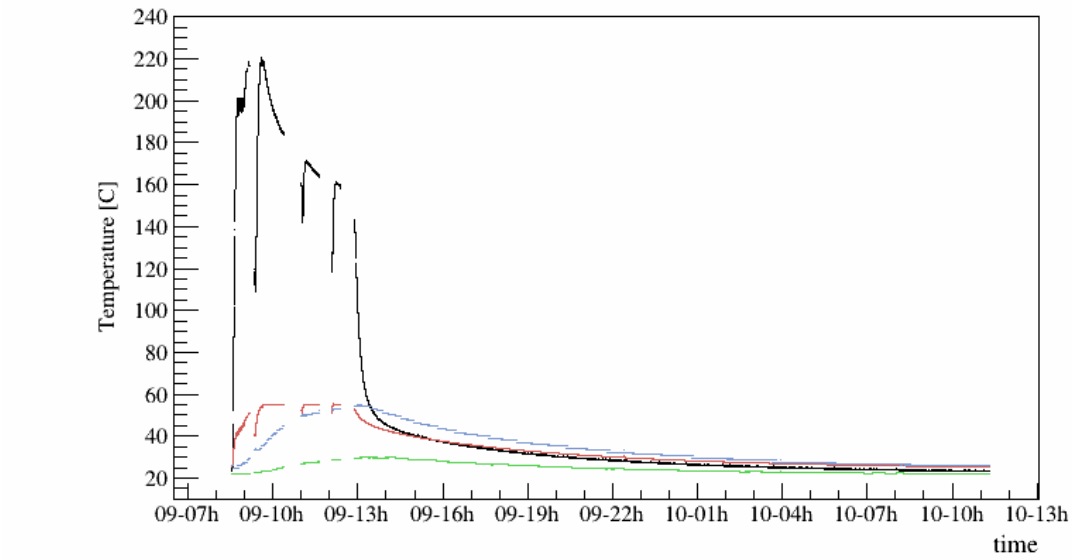

Figure 5.5: Temperature profiles for later heating tests on the test vessel. Red: Inner acrylic surface RTD. Blue: IR Probe aimed at inner surface. Black: Source temperature. Green: Outer AV surface RTD temperature.

5.2 TPB Source Testing

5.2.1 Test Vessel Deposition

The first large scale vacuum deposition on the test vessel[1] was performed on 17 April 2013. After the initial vacuum bake test, 0.883 grams of TPB was loaded into the copper crucible with a target deposition thickness of 1 μm. The source was positioned inside the test vessel on auxiliary cables of a fixed length as this was not a test of the deployment system.

Figure 5.6 shows the thickness of coating as measured from the quartz deposition monitor located in the neck of the test vessel as a function of time. The slow rise

[1]The 20" test vessel is colloquially named "Shallow" by the author, as it is only a little DEAP...

at the beginning was correlated with initial heating of the source, but before the sublimation temperature of TPB (around 208°C) and subsequent evaportation began. The readout from the deposition monitor is calibrated to a deposition medium with density of 1.0 g/cm^3, so a density correction of 1.079 g/cm^3 was applied to plot the true coating thickness. The relevant values from the deposition are summarized in Table 5.2.

parameter	value
TPB loaded [g]	0.883
TPB evaporated [g]	0.883
density corrected final thickness [μm]	0.984
deposition rate [μm/hour]	1.08

Table 5.2: Test TPB deposition parameters

During this deposition, the heater power was manually tuned to give a deposition rate near 1 μm/hour. Fitting the data from Figure 5.6 between 3500 and 6000 seconds results in a deposition rate of 1.08 μm/hour. The deposition rate quickly decreases when the quantity of TPB powder still in the crucible has nearly expired. At this point, the power to the heater was turned off.

Figures 5.7 and 5.8 show the test vessel after TPB coating under visible and UV light. Qualitatively, the entire vessel was successfully coated in TPB; there was no quantitative determination of coating uniformity as direct profile scans could not be performed inside the test vessel. It should be noted that the surface of the vessel prior to deposition was smooth. This smooth finish is not expected in the DEAP-3600 AV, as the coating was applied after resurfacing. Surface roughness features from 1-2 μm are expected from this sanding process.

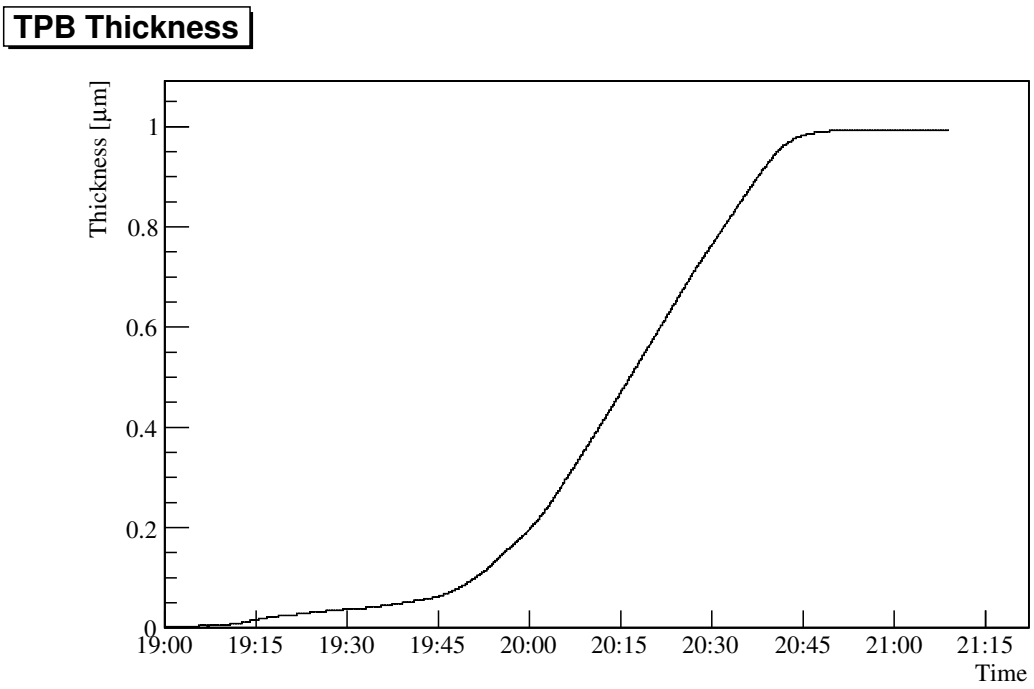

Figure 5.6: Thickness of TPB coating as a function of time as measured in the neck.

5.3 Thickness Monitoring

While the initial TPB test coating was on the test vessel, 4 of the 6 available light guide stubs were populated with extra R5912 PMTs. LED flasher data was taken after the deposition in an effort to independently determine TPB coating thickness. The ultimate goal of this study would be to produce a mapping of the TPB uniformity in the DEAP-3600 vessel. While this data can be collected with the optical calibration source, flashing LEDs during the TPB deposition can shed light on the growth and application of the coating as a function of the deposition time. Details were outlined in Section 3.3.2 for the pulser used in this test.

Figure 5.7: TPB coated test vessel under visible light.

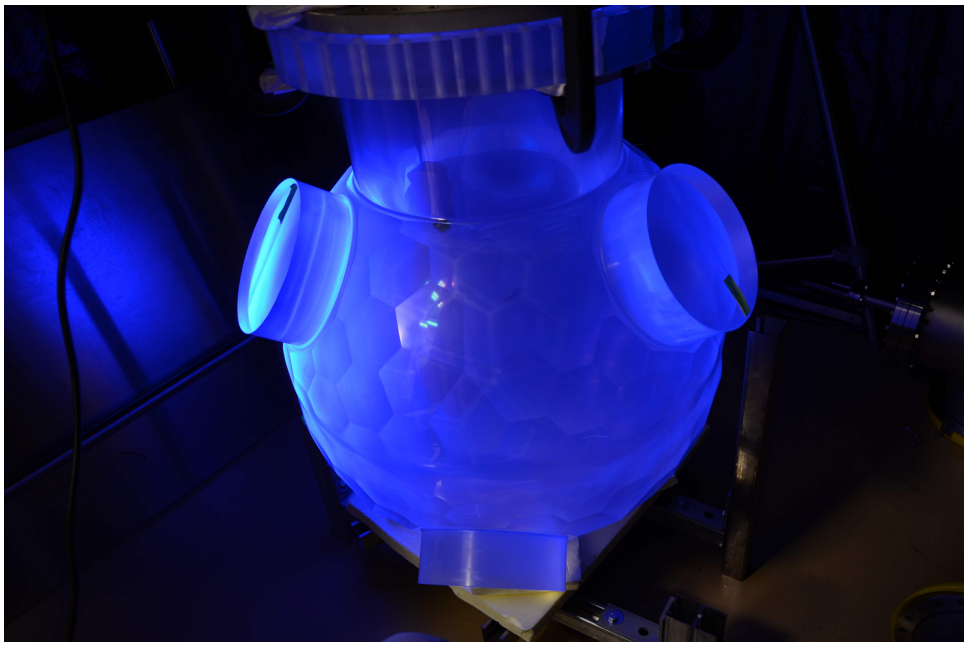

Figure 5.8: TPB coated test vessel under excitation from a UV light. The bright spot on the left light guide stub is due to close proximity of the UV lamp.

5.3.1 Setup

To mimic the optical response setup in DEAP-3600, the test vessel in Figure 5.7 was wrapped in Tyvek as a diffuse reflector. Each R5912 PMT was attached to the light guide stub with aluminum specular reflectors wrapping the stub to funnel light from the vessel into the PMTs. Using extra mounts, each PMT was held to the stub and reflector using band clamps and springs as those used on the DEAP-3600 detector. Coupling between the face of the light guide stub to the front face of the PMT was kept to a minimum, but filled with air; in DEAP-3600 this space is filled with an oil to serve as an optical coupling. The entire setup is contained in a large 2 meter by 2 meter darkened room in the cleanroom at Queen's. An additional large darkening bag was constructed out of black plastic sheeting to cut down on light leaks into the dark box, and fully enclosed the test vessel while allowing PMT cables to pass through the top. Each PMT and mount assembly was additionally wrapped in two layers of black plastic bags and sealed with electrical tape to prevent light leaks from the unused holes in the mounts where optical coupling fluid would be filled. The two additional light guide stubs without PMTs were fitted with aluminum specular reflectors and PMT mounts covered with black plastic. Figure 5.9 shows the fully outfitted test vessel.

Table 5.3 lists the PMTs used on test vessel along with their nominal operational voltages and mounted positions. Limitations in the number of available power supplies required that the PMTs be grouped in pairs. Each power supply has a matched Channel A and B output. Therefore, PWEK and PWAW shared one power supply, while PWEN and PWBE shared another.

Dark rates of 1-5 kHz were attained with the PMTs at an operation voltage of

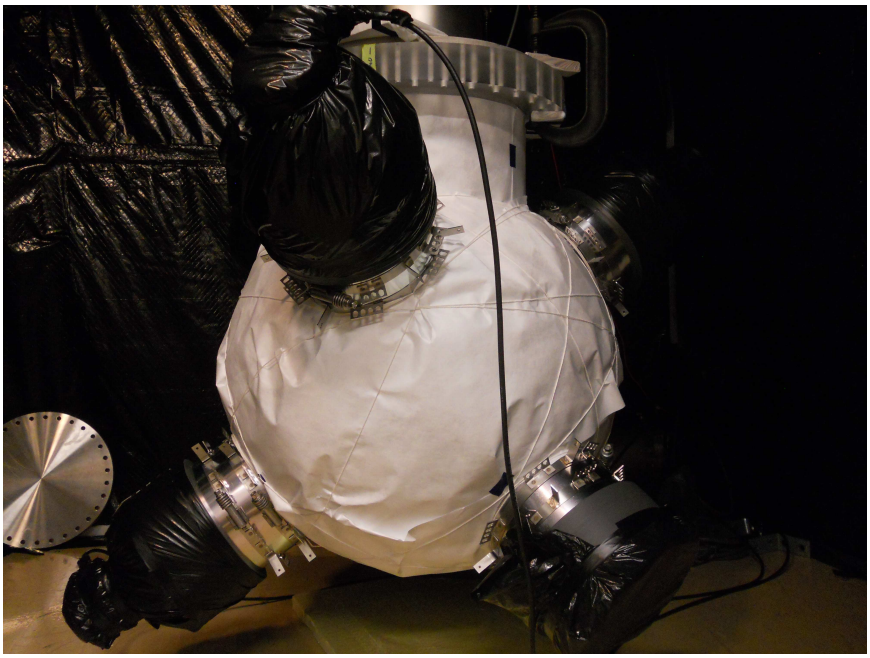

Figure 5.9: Test Vessel wrapped in diffuse reflector and populated with PMTs. Light guide stubs are wrapped in specular reflector and the PMT backs are wrapped in black plastic bags.

Channel	Trace Color	PMT ID	Voltage	Angle
1	Black	PWEK	1612	120°
2	Red	PWAW	1698	0°
3	Green	PWEN	1577	240°
4	Blue	PWBE	1590	300°

Table 5.3: Information on the mounted PMTs on the test vessel.

approximately 1 kV when the dark box was sealed and the room lights dimmed. The additional light reduction bag was put in place as repeated opening of the dark box introduced light leaks near the door. The PMTs were initially set up with signal output sent to a LeCroy WavePro 950 digital oscilloscope with -2 mV trigger threshold.

PMT and triggering cables were fed into the dark box through a baffled U-bend feedthrough. A NIM rack containing high voltage power supplies, logic units, fan-out

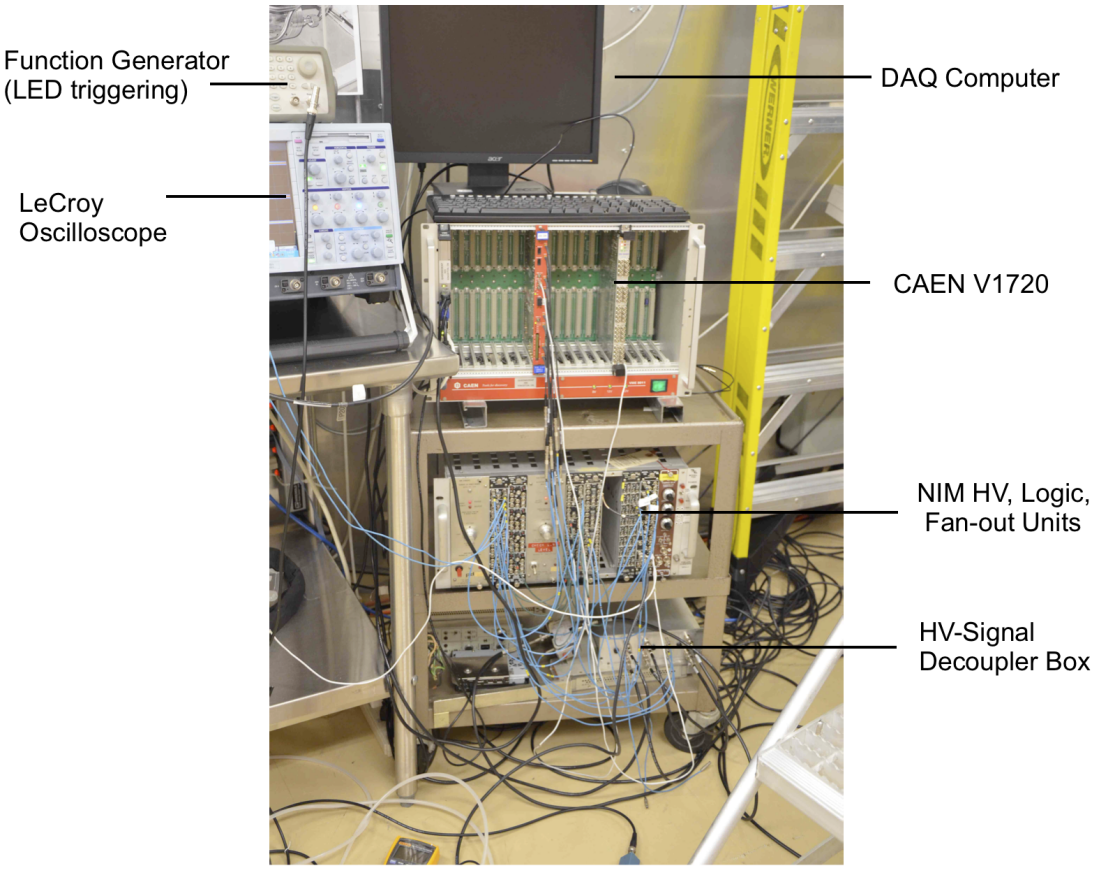

Figure 5.10: DAQ setup used for the TPB thickness test including LeCroy oscilloscope, V1720 interface, and NIM crate.

boards, and a CAEN V1720 digitizer was brought into the cleanroom for the data acquisition system (DAQ). Data from the V1720, digitized in 4 ns bins, was collected using MIDAS software and converted to ROOT files using the DEAP-1 midas2root script. Additional decoupler boxes, which separate the high voltage from the signal returning from the PMT were built. A picture of the DAQ can be seen in Figure 5.10.

The data were analyzed using DEAP-1 analysis software with modifications expanding processing from 2 to 4 PMT channels. This analysis software also corrects

for known single-bin artifacts from the DAQ that are found in the raw traces. The analysis chain for each pulse follows:

1. The baseline of each pulse is found by linearly fitting the early bins in the trace with those at the end of the trace window (pre- and post- signal bins).

2. The peak of each pulse was found by looking for the global minimum (PMT traces are negative).

3. Each PMT trace was shifted in time to align the peak position

4. All triggered pulses are summed together and averaged

5.3.2 Triggered Data

The output from an Agilent 33220A function generator, set to the specifications discussed in Section 3.3.2 was split before being sent into the dark box: one signal was used to generate a NIM trigger for the DAQ, the other was superimposed with a voltage offset and sent to the LEDs in the detector. For simplicity during this test, the LED driver was mounted on the end of a stainless steel pole that could be extracted, and set back into position in the same orientation. Despite this, there was some unavoidable variance in the final orientation and positioning of the LEDs. Data was taken with one stock LED, as well as 2 LEDs driven by the same board that had been diffused. For each LED configuration, data was taken with both the TPB-coated test vessel, and with the TPB coating sanded off. This sanding was performed by hand using the same sandpaper used by the resurfacer on the DEAP-3600 vessel.

After sanding off the initial TPB coating, the test vessel was fully rinsed with UPW three times until the rinse water was clean of acrylic dust. The vessel was then

re-attached to the vacuum system. Care was taken to ensure the orientation of the vessel relative to the vacuum system was the same before sanding. Additionally, the PMTs were carefully replaced in the same rotation with respect to the light guide stub they were attached to prior to sanding. This was to ensure there was no difference in PMT characteristics due to magnetic field interference. The approximately 0.25 gauss field at the Earth's surface can affect the electron transit properties inside the PMT depending on the orientation relative to the field. Later, magnetic shielding was additionally placed around the mounted PMTs to cut down on electric field effects.

The largest uncertainty in this thickness measurement is the final orientation of the LED pulser. The measurement of the overall light collection/attenuation is highly correlated to the angular intensity of the LEDs as viewed by the PMTs. Lack of angular alignment precision contributes largely to the variation in intensity between the collected light per PMT and can be seen in Figure 5.11 from a summed data set with the TPB coating still in the vessel.

Although there is a time delay between the function generator sending the trigger signal to the LEDs and the LEDs firing, that signal propagation time was kept consistent during all data taking. The distance between the LEDs and the PMTs on the test vessel was also kept consistent, and the flight time of the first-arriving photons from the LED pulser to the PMTs is a fraction of the bin width of the DAQ.

The timing offset between TPB and no TPB coating would be small, and a one bin jitter from the DAQ or other non-TPB related sources could complicate interpretation of the data. As the system is not changing during the data taking, offsets due to signal or photon transit times is not expected to change. Still, the necessity for peak alignment (Step 3) in the analysis chain was identified through a jitter in the peak

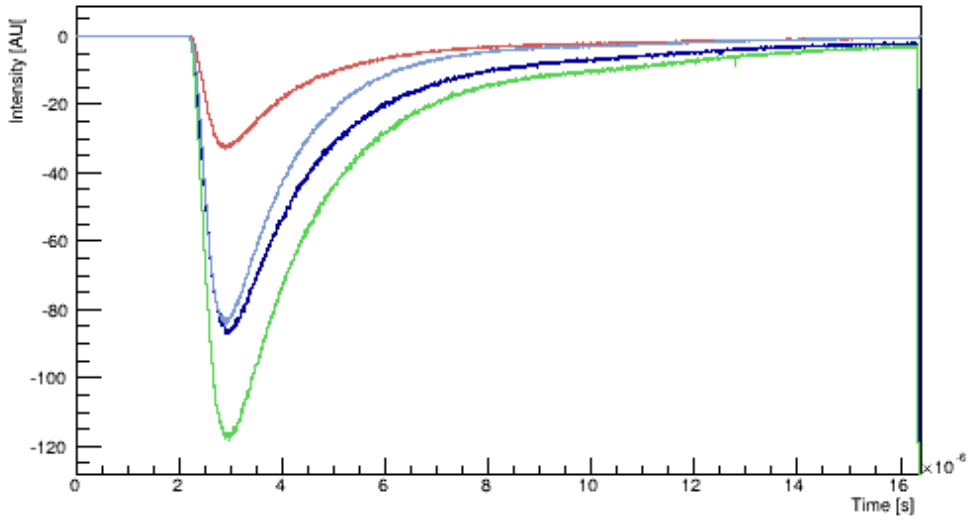

Figure 5.11: 10,000 pulse aligned and summed waveforms collected with TPB coating. Black: Channel 1, 120°. Red: Channel 2, 0°. Green: Channel 3, 240°. Blue: Channel 4, 300°.

time distribution. The distribution of peak times in the data prior to alignment is shown in Figure 5.12.

The collected data with diffused LEDs for TPB and no TPB coating is shown in Figure 5.13. and Table 5.4 summarizes the 20% to 80% rise times for the averaged pulses in each scenario. In the panels of Figure 5.13, the dotted line represents the data taken without TPB coating the test vessel (after sanding), and the solid line represents the data taken with the TPB coating (prior to sanding). The channel colors have been kept consistent across the plots in this section. The ordinate axis for these plots is in units of 4 ns bins. Channel 0 appears to only have one PMT trace, but the data from TPB and no TPB lie on top of each other.

From Table 5.4 there is no noticeable difference between the rise times of the pulses measured with and without TPB coating. The axis of the LEDs is approximately 60°

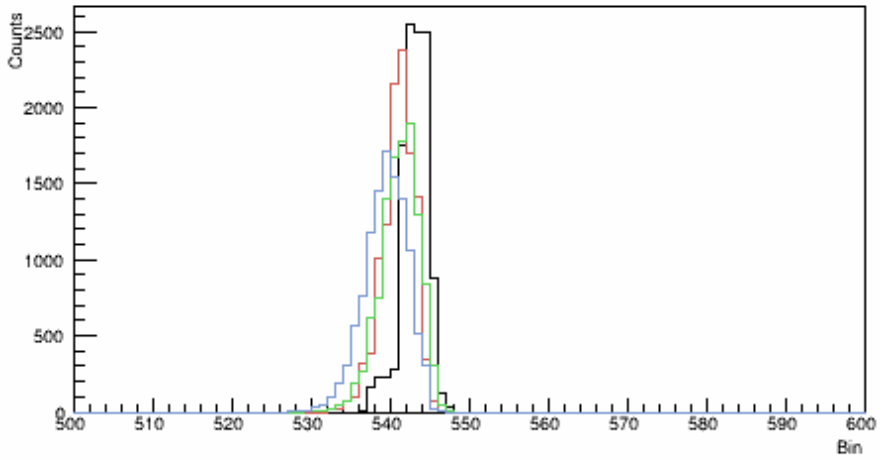

Figure 5.12: Uncorrected pulse peak distributions. Channel colors consistent with Table 5.3

Channel	with TPB	without TPB
1	8 ns	8 ns
2	8 ns	8 ns
3	8 ns	4 ns
4	8 ns	8 ns

Table 5.4: Rise times corresponding to the traces in Figure 5.13.

- 240°. Therefore Channel 2 (red) and Channel 3 (green) were more closely viewing the LEDs on axis and should have been most sensitive to the presence of the TPB coating. However, the average pulse amplitude increases with the coating present in Channel 2 while decreasing in Channel 3. The magnitude of the averaged amplitude is so sensitive to the position of the pulser, that the differences with and without TPB likely arise from mis-alignment of the pulser between the two tests.

Owing to timing in the overall DEAP-3600 construction schedule, difficulty in

creating a sufficiently fast pulse, and the inconsistencies in this data, the TPB source-mounted LEDs were abandoned before either further testing or analysis development could be conducted.

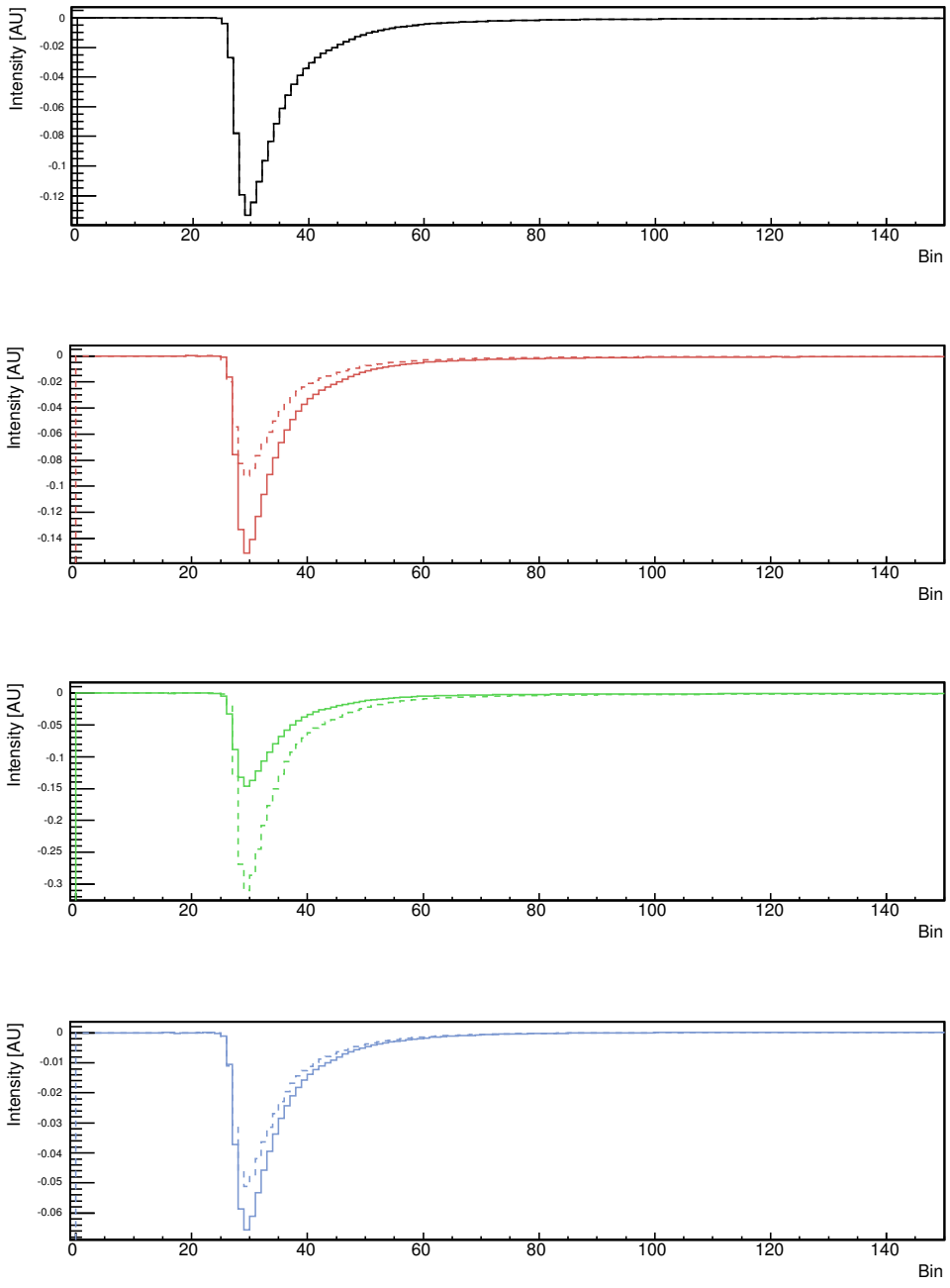

Figure 5.13: 10,000 averaged and pulse aligned pulses. Dashed line: no TPB coating. Solid line: TPB coating. Colors consistent with Table 5.3. The axis of the LED pulser is approximately 240°-60°. Bin widths are 4 ns.

Chapter 6

Final Results

Results of the underground installation of the deployment and deposition systems are presented. Building of the vacuum system in preparation began in January 2015. The bakeout of the acrylic vessel itself began on 18 April 2015 and lasted until 27 May 2015. After this, the source was removed from the AV and filled with TPB powder. Further considerations on the target thickness of the coating (as indicated in Section 3.4) and the limited amount of TPB physically loadable into the crucible lead to two separate depositions, the first beginning on 19 June 2015 and the second on 27 June 2015. After completion of the TPB deposition, the source was removed and the laserball was installed for optical calibration.

6.1 TPB Purity

The purity requirements for DEAP-3600 to see less than 0.1 background events in 3 years running for the TPB are shown in Table 6.1, along with results from two TPB samples that were directly assayed at SNOLAB. For the deposition on DEAP-3600, care was taken to produce and maintain TPB that was as clean as possible, and special accommodations in the production process were made by the supplier, Alfa

Aesar. Although a direct assay of the new TPB was not possible in the time before deposition, a measurement based on surface backgrounds during initial argon gas fill is planned.

		^{210}Po	^{238}U	^{232}Th
< 0.1 events	ppt	5×10^{-9}	0.2	0.8
in 3 years	μBq/kg	15.8	2.4	3.2
Sample	Mass	Source	^{238}U [mBq/kg]	^{232}Th [mBq/kg]
DEAP-12	25.05	Sigma Aldrich	<3.88	< 8.71
DEAP-17	14.7	A&C	<4.33	<1.69

Table 6.1: TPB purity requirements for DEAP-3600, along with direct assay results from 2 samples measured at the SNOLAB underground counting facility

6.2 Surface Preparations

After final machining and cleaning of the TPB source, a small vacuum chamber was set up and the source was baked at 210°C for one week. Following this vacuum baking, the source was allowed to cool under vacuum, then removed from the chamber and immediately heat sealed inside multi-layer DuPont bags. This bagging material, made from thin layers of nylon, aluminum foil, and low density polyethylene, was found by SNO+ Collaboration to have low radon emanation and permeation [42]. The bagged source and crucible was then sealed in a 10" CF tee and shipped underground, where they stayed sealed until installation in the detector.

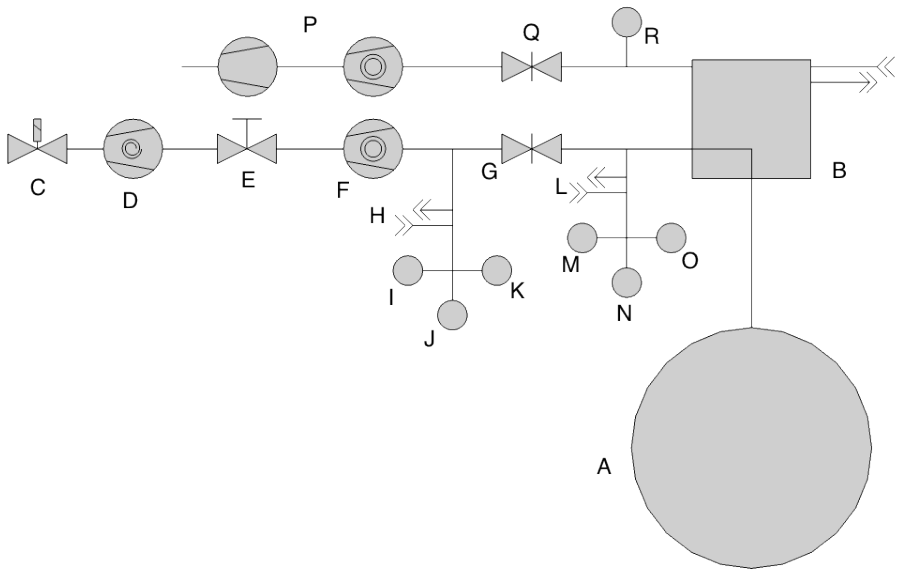

Figure 6.1: Schematic of the vacuum system for AV bakeout and TPB deposition. Components are listed in Table 6.2.

6.3 Underground Preparation

6.3.1 Vacuum System

After extraction of the resurfacer, the AV neck was capped with a purge flange and radon-scrubbed boil-off nitrogen was cycled through the AV. The vacuum system consisted of an inner-glovebox linkage connecting the neck/AV space to the external-glovebox vacuum system. Figure 6.1 shows a schematic of the vacuum system, with the major components listed in Table 6.2.

A 1250 l/s Pfeiffer HiPace turbomolecular pump, backed by an Edwards nXDS 10i scroll pump were connected through 2 10" CF tees to the glovebox wall. A chilled water loop was run from the deck water lines to cool the TMP. Dividing these two

Designation	Component
A	Acrylic Vessel Volume
B	Glovebox Volume
C	Solenoid Ballast Control
D	nXDS 10i Scroll Pump
E	KF40 Isolation Valve
F	Pfeiffer HiPace 1250l/s TMP
G	10” CF GTMP-8002 NorCal gatevalve
H	Turbo Leg N2 Purge In/Purge Out
I	Pfeiffer PKR Vacuum Gauge
J	Omega Pressure Gauge
K	Omega Pressure Gauge for Latching Power Controller
L	AV N2 Purge In/Purge Out
M	Pfeiffer PrismaPlus RGA
N	Pfeiffer PKR Vacuum Gauge
O	Baratron Pressure Transducer
P	Pfeiffer HiCube Pumping Station (TMP and roughing pumps)
Q	2.75” CF Gatevalve
R	Pfeiffer PKR Vacuum Gauge
S	Glovebox N2 Purge In/Purge Out

Table 6.2: List of vacuum components as shown in 6.1

tees was a 10” CF GTMP-8002 NorCal gatevalve, used to isolate the AV and pump in the event of a power failure or spike in pressure. Each tee had installed a Pfeiffer PKR vacuum gauge, as well as a low vacuum gauge. Additionally, each tee had purge inlet and outlet lines: the AV side for purging the AV directly, and the turbo side for purging after the system had been closed with the gatevalve. A controllable solenoid was installed on the ballast valve of the scroll pump for remote adjustment. It was found after pumping on the acrylic, that water was condensing in the scroll pump and reducing its pumping capacity. Periodic burping of the ballast was required to remove this water from the pump. Finally, a Pfeiffer PrismaPlus RGA was installed on the AV side of the gatevalve through an all-metal valve, though this was not used

during the bakeout.

All components were driven through two uninterruptible power supplies capable of surviving power fluctuations and brief planned power outages underground. As the integrity of the AV was of utmost importance, the system was designed to isolate the AV from the vacuum pumps with the 10" CF gatevalve in the event of a power issue or pressure spike. In the former case, the gatevalve would shut to prevent lab air from streaming back into the AV from an unpowered pump, and in the latter, power was cut from the turbo to prevent its exposure to near-atmospheric pressure while at full rotation. After any fault resulting in tripped power, a latching machine switch would maintain the system in a powered-down state and prevent run-away conditions even if the power returned, forcing operators to be present to safely and controllably restart the vacuum system.

The linking piece that connected the AV and neck space to the vacuum system on the exterior of the glovebox, was a custom 10" CF - 12" CF 5 way cross (5WC), designed and specified for use with the original deployment system. Installation of the 5WC was done in the glovebox under nitrogen purge, as the post-resurfaced AV was directly exposed during this step.

Installation of the 5WC became highly non-trivial, and the system seemed to never fully seal the AV from the mine air. As a result, the glovebox was kept shut and continually purged prior to pumping on the AV. During evacuation of the AV, a second pump system was used to pull a vacuum on the glovebox. The leak rate from the AV into the glovebox was proportional to the pressure differential between those two volumes. Therefore, pumping simultaneously on each volume and keeping the pressure differential as low as possible mitigated the leak between the two volumes

and helped attain the necessary overall vacuum in the AV.

A leak between the steel shell and glovebox was later found when purge gas from the steel shell was visible in the glovebox RGA scans. However, upon extraction of the 5WC, two further issues were noticed. Firstly, the o-ring seal between the 5WC and bellows was rolled in the retaining ring groove, likely due to the tight installation tolerances. Secondly, the knife edge surface on the same flange was damaged, presumably during installation, which could have limited the sealing capacity of the o-ring.

6.3.2 Source Assembly

Assembly of the deployment system underground was carried out in a clean tent in the Cryopit at SNOLAB. Before transportation from the clean tent to the Cube Hall for installation into the detector, a bag was created to cover the entire length of the deployment pipe and limit its exposure to lab dust.

Because the source was baked at high temperature before being bagged and shipped underground, exposure to mine air was to be kept at a minimum to prevent further radon exposure. However, owing to the difficulty of working in the glovebox, and the fragility of the temperature sensors mounted on the source surface, the source was removed from Dupont liner bags and initially wired and attached to the deployment pipe in lab air. The allowable exposure of the source to mine air was calculated from:

$$t \times \rho \times \frac{0.001\text{Bq/m}^2\ ^{210}\text{Po}}{\text{year Bq}\ ^{222}\text{Rn}} \times A \tag{6.1}$$

for t the time the stainless steel is exposed to lab air, ρ the radon concentration

120 Bq/m^3, and A the surface area of the source. For a one hour exposure, this results in 1.04×10^{-6} Bq or 1.04 μBq ^{210}Po. The full radio-purity budget for the TPB system in the AV was set at 22 mBq for 1 week exposure to the AV, or 5 mBq for 1 month exposure.

6.3.3 Slow Controls Modification

After installation of the source, an apparent grounding between the RTDs and chassis was noticed. This prevented proper RTD readout with the intended LakeShore monitor. To solve this issue, the temperature sensors were read out with the DeltaV slow controls system. Additionally, the heater power control was reconfigured to be controllable through the DeltaV. A custom online interface with pressure, temperature, and power readings was created and the data logged. This allowed for remote operation of the heater during the AV bakeout. With the capability to generate a 4-20 mA control signal directly from the DeltaV, the 0-10 V control signal was no longer necessary. The converter was then bypassed in the electrical box.

As the DeltaV cannot directly measure resistances, but voltage, an ad hoc interface was made by reading the voltage across the RTD using the circuit in Figure 6.2. Changes in resistance of the RTD due to temperature, which follows Equation 6.2, would effect the voltage drop across the circuit

$$R(t) = R_0(1 + at + bt^2) \tag{6.2}$$

for $R_0 = 100\,\Omega$ for PT-100 RTDs, $a = 3.91 \times 10^{-3}$, and $b = -5.80 \times 10^{-7}$, and t the temperature in Celsius. The right branch in Figure 6.2 was used to correct for drifts in the power supply voltage. The labeled nodes indicate connection points to

the DeltaV.

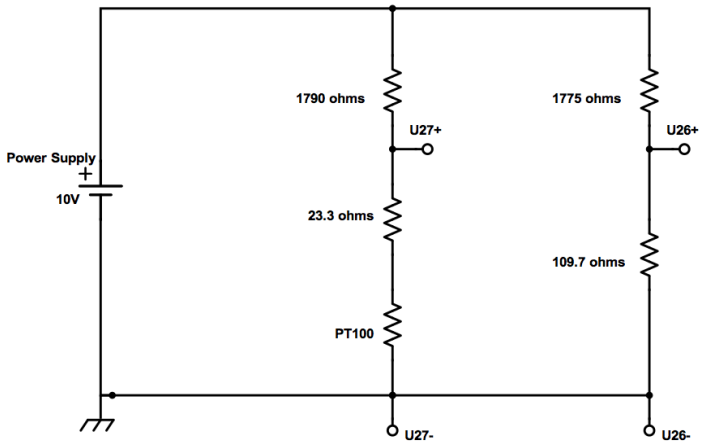

Figure 6.2: Readout circuit for the source RTDs with DeltaV.

6.4 AV Vacuum Bake

Vacuum baking of the AV, originally estimated to take a week, lasted nearly 6 weeks. Although initial modifications to the RTD readout were successful, it quickly became apparent that less heating power was being delivered from the source than expected. In the final cleaning steps for the source, it was baked above 200°C in a small vacuum chamber. The 200°C upper temperature limit was set by the temperature rating on the Kapton insulated RTD wires and a section of Teflon heat shrink around the heating element's contact wire leads. To achieve this source temperature in the bake, the duty cycle from the power relay was at nearly 100%, or close to the 275 W power limit of the heater itself.

A flicker in the readout value of the RTDs was noticed on a few occasions during the AV bake and TPB deposition. In one example, shown in Figure 6.3, a drop in the temperature of the source can be seen at 01:00 on 28 July. If this flicker is the result

of a connection issue between the DeltaV and RTD on the source manifesting itself with a 10 Ω− 20 Ω offset, the discrepancy in the expected output power for the source may be resolved. An unaccounted for 10 Ω resistance offset corresponds to reading the temperature approximately 20°C higher than the true value. An apparent power of 160 W, scaled by this offset, approximately recovers the 275 W expected running power.

The RTD leads are very flexible and are connected at the end of an effective 4 meter arm. Any shaking of the experimental supporting deck (which does occur) could induce a pendulum effect causing the source to slightly sway. Any movement of the source would stress the connection at the RTD leads; momentary shorting/unshorting due to stressing of the RTD leads is not unimaginable and was seen during maintenance wiring inside the glovebox prior to deployment.

A number of attempts were made to speed up the heating of the AV. Low pressure nitrogen gas was added into the AV to act as a buffer, but concerns over stress in the acrylic due to uneven heating drew this attempt to a halt. The warm gas convection inside the AV was heating the neck region more than the south pole, as viewable by the inner-most RTDs attached to the filler blocks. Stresses in the neck region were of most concern. Eventually, external heat was applied to the steel shell, first by closing off the shield tank and circulating lamp-warmed air, and then by turning off the air conditioning to the Cube Hall.

At the end of the bakeout, the inner-most ring of temperature sensors, which are a distance of 6.7 cm from the inner surface of the acrylic, achieved and average value of 43°C. A conservative 5 degree increase, backed by finite element analysis by C. Ng, extrapolates the inner surface temperature close to the targeted 50°C. The baseline

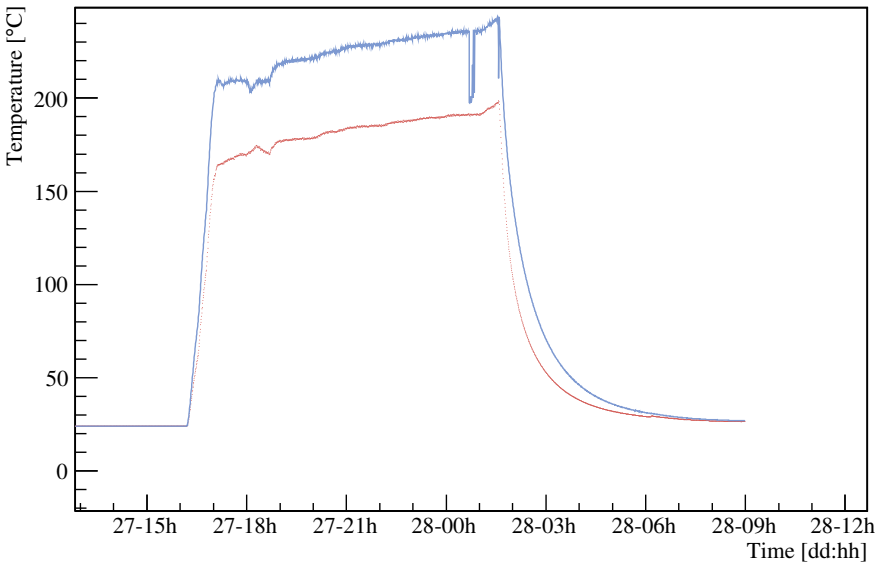

Figure 6.3: Source temperature during the second TPB deposition. A ~ 20°C flicker in the readout around 01:00 on 28 July could be indicative of a mis-reading of the source temperature.

pressure gauge reading before baking out the AV was 2×10^{-5} mbar, and after baking was 7×10^{-6} mbar. This drop in attainable pressure indicates a removal of absorbed water in the acrylic surface. In the end, the gas load from the AV was limited by bulk diffusion.

In the vacuum system geometry, the pressure gauges were far from the AV volume itself, and were connected to the main vacuum line through relatively poor conduction branches. A monte-carlo based simulation package, Molflow, was used to predict the AV pressure relative to the gauge readings. From this, the gauge pressure readings were found to be approximately a factor of 2 lower than the AV vacuum.

As outlined in Chapter 3, the AV vacuum is directly linked to the achievable mean

free path of the TPB molecules after leaving the source. There are some conservative estimates built into the calculation of the desirable AV pressure, notably the diameter of the TPB molecule, set at 1220 pm, which is taken from the longest diagonal span across the molecule. A mean free path of 0.85 m corresponds to a vacuum in the AV of 1.16×10^{-5} mbar. A gauge-corrected pressure of 1.4×10^{-5} mbar was achieved, yielding a mean free path around 0.7 m. Because of the conservative estimate of the diameter, d, of the molecule, which scales the mean free path as $1/d^2$, this achievable vacuum was deemed acceptable for the deposition of the TPB.

6.5 TPB Deposition

Prior to insertion in the detector, the filled TPB source was baked inside the glovebox. Following the surface preparations in [37], the TPB powder was brought to 150°C for 2 hours. To achieve this, the glovebox and canister were pumped to a rough vacuum of 50 mbar to better the thermal transfer between the source and the crucible. After each prebake, the source was allowed to cool under vacuum, purged back to atmospheric pressure with radon-scrubbed boil-off nitrogen, and then final configurations were made to the sensors before redeployment inside the AV. The AV was pumped down to a base pressure around 8×10^{-6} mbar, as read from the AV-side vacuum gauge, before each deposition.

Two evaporations, 14.0 ± 0.1 g and 15.4 ± 0.1 g by mass, were performed on the DEAP-3600 acrylic vessel. The target evaporation rate was aimed at 1 Å/s. First demonstration of a stable deposition rate can be seen in Figure 6.4 from the deposition on 19 June 2015. Unfortunately, the deposition monitor signal became unusably noisy, and a direct thickness measurement for the first deposition could not

be made. Applying a linear fit to the stable thickness increase yields a deposition rate of 0.70 Å/s.

The nominal input power into the heater from the AV bakeout (i.e. with the TPB source empty) was 150 W. At the beginning of TPB deposition, the input power required to maintain a crucible temperature of 200°C was 220 W. When the TPB in the crucible became exhausted, less input power became required, falling from 220 W back to 150 W. As the TPB is evaporated, the extra heat load is removed, and the crucible-source system begins to act like the empty source from the AV bakeout. This was further indication, despite having lost the direct thickness measurement with the quartz crystal in the first deposition, that the evaporation was over. Nevertheless, the heater was run for a few hours past the estimated full deposition time to ensure that all the TPB had been evaporated away.

The thickness plot for the second deposition, which occurred on 27 June 2015, can be see in Figure 6.5. Here, a stable deposition rate of 0.69 Å/s was achieved.

Indications of incorrect reading of the RTDs was again apparent during the second deposition. The deposition rate of TPB as recorded from the monitor was lower than previously seen during the heating of the source. A longer initial heating and a slower increase of the power was taken to conservatively address this issue. The final operating temperature of the source was eventually driven to achieve a similar deposition rate and performance to that of the first deposition.

In both depositions, the crucible's entire contents were emptied during the evaporation in the AV. The combined total mass deposited was 29.4 ± 0.2 g. Over the 9.10 m^2 inner surface area of the AV this would yield a uniform coating thickness of 3.00 $\pm$ 0.02 μm. Using the full data set from the deposition monitor during the second

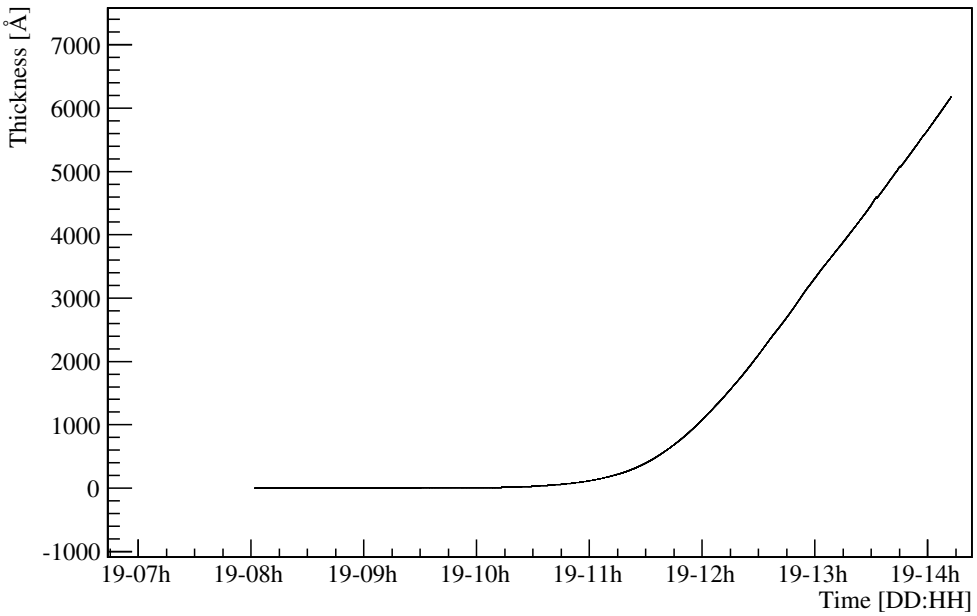

Figure 6.4: Thickness as a function of time measured for the first TPB deposition.

deposition, a 15.4 g mass would uniformly develop a 1.57 μm thick coating. There is a 23% error between this value and the thickness reading of 1.21 μm. However, in the relative position of the deposition monitor with respect to the source there may have been some shadowing of the monitor due to the coiled power cables running to the source, as well as the deployment pipe itself. Scaling the second deposition thickness value by the ratio of mass loaded into the crucible, the extrapolated first deposition thickness becomes 1.09 μm. Figure 6.6 shows this extrapolation (dashed blue), the useable first deposition data (solid blue), and the full second deposition thickness curve (green). The extrapolated total thickness then becomes 2.30 μm, as opposed

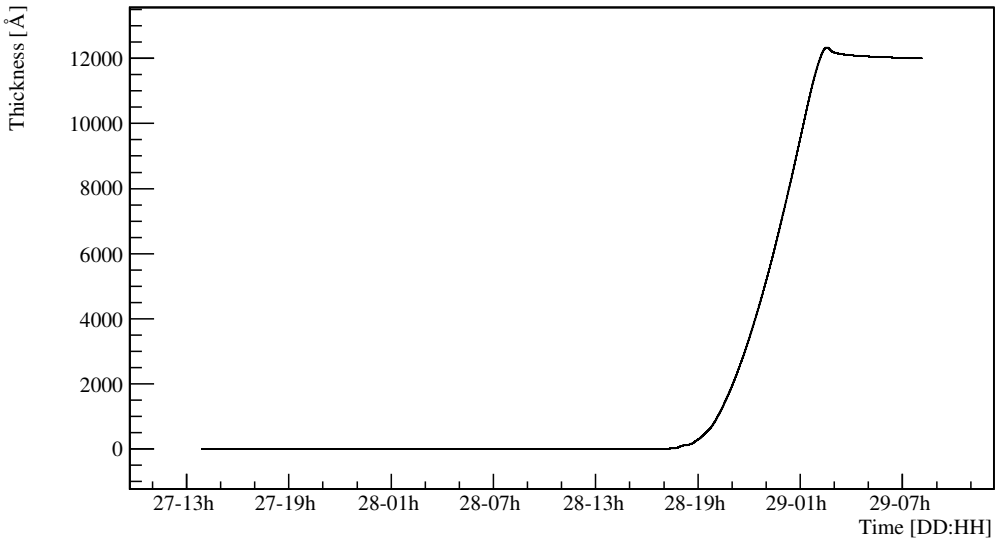

Figure 6.5: Thickness as a function of time measured for the second TPB deposition.

to the 3.00 μm predicted by mass. Given the potential shadowing effect and thickness extrapolation, these two values agree within a few percent to the 20% thickness non-uniformity target. Further hopes of understanding the coating thickness lie in uniformity analyses based on optical and background data, which are ongoing.

After completion of the depositions, the source was extracted and the deployment system rebuilt for use with the fibre-driven LaserBall. The 3 acrylic witness samples were removed from the stage and stored in a dark box for transportation back to Queen's for surface analysis. Figure 6.3 show two samples, briefly illuminated with an ultraviolet lamp for qualitative examination of the coating quality. The circular feature on each disk is a region uncoated with TPB, that was under a washer used in mounting the disk to the underside of the stage. To eye, there were no issues

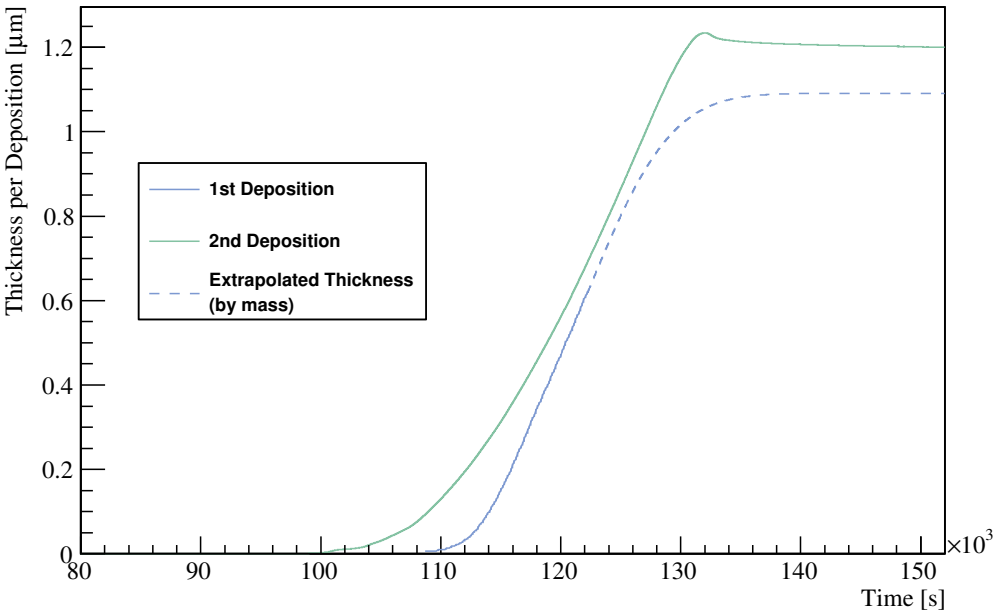

Figure 6.6: TPB thickness per deposition. Blue: first deposition thickness curve and extrapolated (by mass) final value. Green: full second deposition thickness curve.

in the coating on the center of the disks. However, edge effects due to handling and mounting could be seen. These features have also been seen on slides during depositions in the Queen's test setup.

6.6 Uniformity Estimation

An early estimation of the TPB uniformity was made using a small data set from runs 010497 and 010502. Both of these were after the second TPB deposition and during purging of the AV with nitrogen. Out of this data set, events generating more

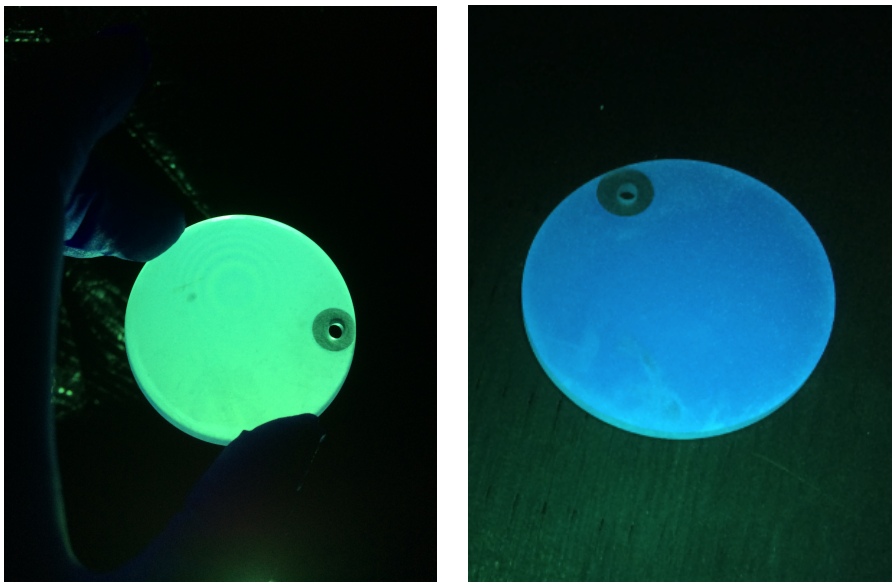

Table 6.3: The 2 sanded acrylic witness samples, briefly examined under an ultraviolet lamp.

than 2000 photoelectrons (PE) were selected. These high PE events likely come from decaying radon emanating from the TPB source inside the vessel, and generate light in the entire detector, though the pressure of the nitrogen purge gas is not the same from run to run. The number of pulses seen per PMT were summed and the total corrected for the individual PMT efficiency, shown in Figure 6.7. Channels 65 (broken) and 119 (dead) were removed from this analysis. Of the 133 events considered, an average of 2235 pulses were seen in each PMT, with a standard deviation of 374 pulses. This yields a uniformity in response of 16.7%, which even for this low statistics sample, corroborates a thickness non-uniformity within target of 20%.

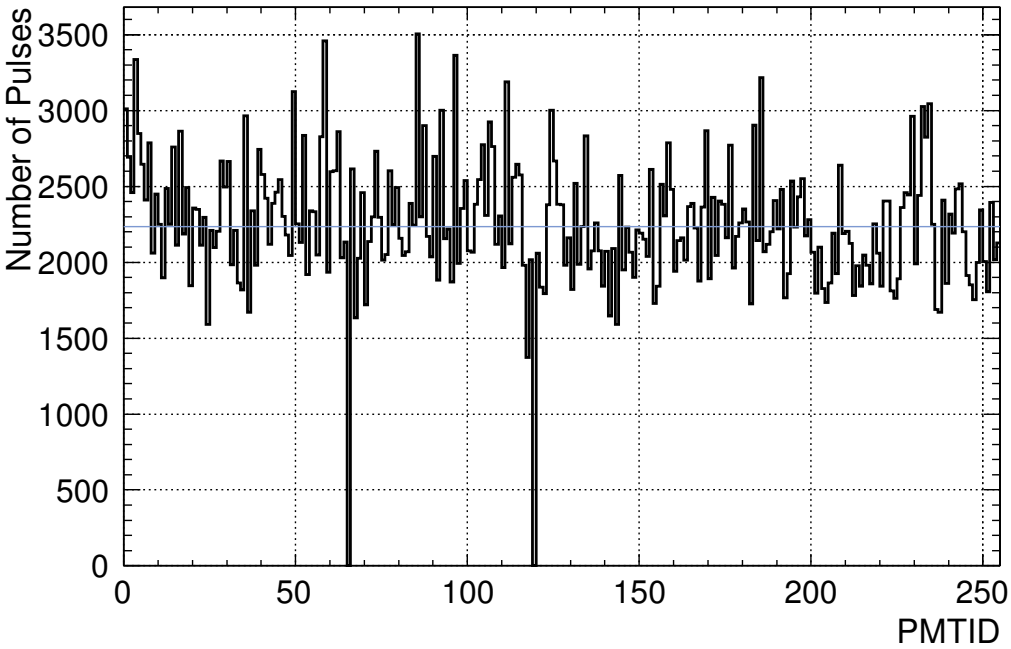

Figure 6.7: Number of pulses seen per PMT for 133 events, 2000PE or greater. The blue line indicates the average across all PMTs. Uniformity in thickness of 16.7% is observed.

Chapter 7

Conclusions

Despite much experimental effort, clarification in the dark matter problem continues to elude the physics community. DEAP-3600 has the potential to perform the most sensitive dark matter search to date, probing further into the parameter space than has yet been attainable. Utilizing 3600 kg of liquid argon as a target medium, vacuum ultraviolet scintillation light from the de-excitation of argon dimers produced from particle interactions is recorded. Wavelength shifting is necessary due to the efficient absorption of ultraviolet photons in optical media, preventing the transmission of event information from the target volume to the photomultiplier tubes. Application of the organic wavelength shifter 1,1,4,4-tetraphenyl-1,3-butadiene to the interior of the acrylic vessel was performed with a custom vacuum deposition system. It is the TPB layer that will allow the DEAP detector to have increased sensitivity to, and potentially discover, dark matter. Adherence to radio-purity requirements for all components entering the post-resurfaced acrylic vessel was necessary to keep radioactive background levels to a minimum. Construction of the DEAP-3600 experiment is now nearly complete.

Extensive work on the development and testing of the TPB deposition source was

undertaken. Additionally, multiple methods for source deployment were investigated and developed. Successful application of the organic wavelength shifter TPB was performed with the system developed for the DEAP-3600 dark matter search experiment. Two vacuum depositions, totaling 29.4 $\pm$ 0.2 g, were performed on the 9.10 m^2 inner surface of the DEAP-3600 acrylic vessel yielding a thickness of 3.00 $\pm$ 0.02 μm by mass. At an ambitious scale for evaporative deposition, early analyses show non-uniformity in the coating thickness to less than 20% across the detector.

Bibliography

[1] F. Zwicky, "Die rotverschiebung von extragalaktischen nebeln," *Helvetica Physica Acta*, vol. 6, pp. 110–127, 1933.

[2] F. Zwicky and A. K. (Ed.), "Republication of: The redshift of extragalactic nebulae," *Gen. Relat. Gravit.*, vol. 41, pp. 207–224, 2009.

[3] P. Collaboration *et al.*, "Planck 2015 results. xiii. cosmological parameters," *arXiv preprint arXiv:1502.01589*, 2015.

[4] L. Bergström, "Dark matter candidates," *New Journal of Physics*, vol. 11, no. 10, p. 105006, 2009.

[5] G. R. Blumenthal, S. Faber, J. R. Primack, and M. J. Rees, "Formation of galaxies and large scale structure with cold dark matter," 1984.

[6] E. Figueroa-Feliciano, "Direct detection searches for wimp dark matter," *Progress in Particle and Nuclear Physics*, vol. 66, no. 3, pp. 661–673, 2011.

[7] R. W. Schnee, "Introduction to dark matter experiments," *arXiv preprint arXiv:1101.5205*, 2011.

[8] J. Lewin and P. Smith, "Review of mathematics, numerical factors, and corrections for dark matter experiments based on elastic nuclear recoil," *Astroparticle Physics*, vol. 6, no. 1, pp. 87–112, 1996.

[9] R. Bernabei, P. Belli, F. Cappella, R. Cerulli, C. Dai, A. dAngelo, H. He, A. Incicchitti, H. Kuang, X. Ma *et al.*, "New results from dama/libra," *The European Physical Journal C-Particles and Fields*, vol. 67, no. 1, pp. 39–49, 2010.

[10] R. Bernabei, P. Belli, F. Cappella, V. Caracciolo, R. Cerulli, C. Dai, A. dAngelo, A. Di Marco, H. He, A. Incicchitti *et al.*, "No role for muons in the dama annual modulation results," *The European Physical Journal C*, vol. 72, no. 7, pp. 1–12, 2012.

[11] M. Boulay, D. Collaboration *et al.*, "Deap-3600 dark matter search at snolab," in *Journal of Physics: Conference Series*, vol. 375, no. 1. IOP Publishing, 2012, p. 012027.

[12] F. Duncan, A. Noble, and D. Sinclair, "The construction and anticipated science of snolab," *Annual Review of Nuclear and Particle Science*, vol. 60, no. 1, p. 163, 2010.

[13] M. Boulay and A. Hime, "Technique for direct detection of weakly interacting massive particles using scintillation time discrimination in liquid argon," *Astroparticle Physics*, vol. 25, no. 3, pp. 179–182, 2006.

[14] "Deap-3600 conceptual design report," 2011, sLDO-DEC-TR-0016.

[15] N. Thonnard and G. Hurst, "Time-dependent study of vacuum-ultraviolet emission in argon," *Physical Review A*, vol. 5, no. 3, p. 1110, 1972.

[16] E. Aprile, A. E. Bolotnikov, A. I. Bolozdynya, and T. Doke, *Noble gas detectors*. John Wiley & Sons, 2007.

[17] M. Schumann, "Dark matter search with liquid noble gases," *arXiv preprint arXiv:1206.2169*, 2012.

[18] T. Doke, A. Hitachi, J. Kikuchi, K. Masuda, H. Okada, and E. Shibamura, "Absolute scintillation yields in liquid argon and xenon for various particles," *Japanese journal of applied physics*, vol. 41, no. 3R, p. 1538, 2002.

[19] M. Suzuki and S. Kubota, "Mechanism of proportional scintillation in argon, krypton and xenon," *Nuclear Instruments and Methods*, vol. 164, no. 1, pp. 197–199, 1979.

[20] M. Boulay, B. Cai, M. Chen, V. Golovko, P. Harvey, R. Mathew, J. Lidgard, A. McDonald, P. Pasuthip, T. Pollman *et al.*, "Measurement of the scintillation time spectra and pulse-shape discrimination of low-energy beta and nuclear recoils in liquid argon with deap-1," *arXiv preprint arXiv:0904.2930*, 2009.

[21] P.-A. Amaudruz, M. Batygov, B. Beltran, J. Bonatt, M. Boulay, B. Broerman, J. Bueno, A. Butcher, B. Cai, M. Chen *et al.*, "Deap-3600 dark matter search," *arXiv preprint arXiv:1410.7673*, 2014.

[22] V. Gehman, S. Seibert, K. Rielage, A. Hime, Y. Sun, D.-M. Mei, J. Maassen, and D. Moore, "Fluorescence efficiency and visible re-emission spectrum of tetraphenyl butadiene films at extreme ultraviolet wavelengths," *Nuclear Instruments and Methods in Physics Research Section A: Accelerators, Spectrometers, Detectors and Associated Equipment*, vol. 654, no. 1, pp. 116–121, 2011.

[23] C. Lally, G. Davies, W. Jones, and N. Smith, "Uv quantum efficiencies of organic fluors," *Nuclear Instruments and Methods in Physics Research Section B: Beam Interactions with Materials and Atoms*, vol. 117, no. 4, pp. 421–427, 1996.

[24] T. Pollmann, M. Boulay, and M. Kuźniak, "Scintillation of thin tetraphenyl butadiene films under alpha particle excitation," *Nuclear Instruments and Methods in Physics Research Section A: Accelerators, Spectrometers, Detectors and Associated Equipment*, vol. 635, no. 1, pp. 127–130, 2011.

[25] I. Berlman, *Handbook of florescence spectra of aromatic molecules*. Elsevier, 1971.

[26] P. V. GmbH, "The vacuum technology book," *www.pfeiffer-vacuum.com/*, vol. 2, 2013.

[27] T. Pollmann, "Alpha backgrounds in the deap dark matter search experiment," 2012, ph.D. thesis, Queen's University.

[28] M. Boulay, "Deap-str-2011-002 radon emanation from welds and process tubing for the deap-3600 argon process system," 2011, internal document.

[29] G. Sauerbrey, "Verwendung von schwingquarzen zur wgung dnner schichten und zur mikrowgung," *Zeitschrift fr Physik*, vol. 155, no. 2, pp. 206–222, 1959. [Online]. Available: http://dx.doi.org/10.1007/BF01337937

[30] V. Mecea, R. Bucur, and E. Indrea, "On the possibility of thin film structure study with a quartz crystal microbalance," *Thin Solid Films*, vol. 171, no. 2, pp. 367–375, 1989.

[31] Inficon, "Sqm 242 thin film deposition controller operating manual," 2011.

[32] J. Kapustinsky, R. DeVries, N. DiGiacomo, W. Sondheim, J. Sunier, and H. Coombes, "A fast timing light pulser for scintillation detectors," *Nuclear Instruments and Methods in Physics Research Section A: Accelerators, Spectrometers, Detectors and Associated Equipment*, vol. 241, no. 2, pp. 612–613, 1985.

[33] M. Ward, personal Correspondence.

[34] P. Amram, M. Anghinolfi, S. Anvar, F. Ardellier-Desages, E. Aslanides, J.-J. Aubert, R. Azoulay, D. Bailey, S. Basa, M. Battaglieri *et al.*, "The antares optical module," *Nuclear Instruments and Methods in Physics Research Section A: Accelerators, Spectrometers, Detectors and Associated Equipment*, vol. 484, no. 1, pp. 369–383, 2002.

[35] M. Kuźniak and T. Pollmann, "Equipment specification: Deap-3600 tpb applicator," Queen's University, Tech. Rep., 2012, qUDO-DEC-SP-6300-00.

[36] D. Gastler, E. Kearns, A. Hime, L. C. Stonehill, S. Seibert, J. Klein, W. H. Lippincott, D. N. McKinsey, and J. A. Nikkel, "Measurement of scintillation efficiency for nuclear recoils in liquid argon," *Physical Review C*, vol. 85, no. 6, p. 065811, 2012.

[37] P.-A. Amaudruz, M. Batygov, B. Beltran, K. Boudjemline, M. Boulay, B. Cai, T. Caldwell, M. Chen, R. Chouinard, B. Cleveland *et al.*, "Radon backgrounds in the deap-1 liquid-argon-based dark matter detector," *Astroparticle Physics*, vol. 62, pp. 178–194, 2015.

[38] M. Boulay, "Deap-3600 acrylic vessel annealing plan," dEAP-STR-2012-013.

[39] "Deap-3600 av vacuum bakeout," 2015, dEAP-SOP-704 rev2.

[40] R. Elsey, "Outgassing of vacuum materials-ii," *Vacuum*, vol. 25, no. 8, pp. 347–361, 1975.

[41] P. Vacuum, "Working with turbo pumps."

[42] M. Seddighin, "Low energy 8b solar neutrinos in sno+: Controlling and constraining radon backgrounds," Master's thesis, Queen's University, 2013.